# Industrial Study for Therapeutic Application of Bacteriophage against *Staphylococcus aureus*

January 2023

Ippei TAKEUCHI

# Industrial Study for Therapeutic Application of Bacteriophage against *Staphylococcus aureus*

A Dissertation Submitted to
the Graduate School of Science and Technology,
University of Tsukuba
in Partial Fulfillment of Requirements
for the Degree of Doctor of Philosophy in Biotechnology
Doctoral Program in Bioindustrial Sciences,
Degree Programs in Life and Earth Sciences

Ippei TAKEUCHI

# CONTENTS

# TABLES

# FIGURES

# ABBRIVIATIONS

Bacteriophage: phage

BDI: Bacterial Density at Infection

BHI: Brain-Heart Infusion

CFU: Colony Forming Unit

CQA: Critical Quality Attribute

DoE: Design of Experiment

DSD: Definitive Screening Design

EOP: Efficiency of Plating

*E. coli*: *Escherichia coli*:

GlcNAc: *N*-acetylglucosamine

GMP: Good Manufacturing Practice

ICH: International Council for Harmonisation of Technical Requirements for Pharmaceuticals for Human Use

IMAC: Ion Affinity Chromatography

IPTG: Isopropyl β-D-1-thiogalactopyranoside

LB: Luria-Bertani

LPS: LipoPolySaccharide

LTA: LipoTeichoic Acids

MOI: Multiplicity of Infection

$OD_{600}$: Optical density at 600 nm

$OD_{660}$: Optical density at 660 nm

OD: Optical Density

ORF: Open Reading Frame

PBS: Phosphate Buffered Saline

PEG: Polyethylene Glycol

PCR: Polymerase Chain Reaction

PFU: Plaque Forming Unit

QTPP: Quality Target Product Profile

qPCR: quantitative PCR

RBP: Receptor-Binding Protein

QbD: Quality-by-Design

SD: Standard Deviation

SDS-PAGE: Sodium Dodecyl Sulfate-PolyAcrylamide Gel Electrophoresis

SM: Sodium Magnesium

*S. aureus*: *Staphylococcus aureus*

MRSA: Methicillin-Resistant *Staphylococcus aureus*

ND: Not Detected

ns: not significant

TEM: Transmission Electron Microscopy

TSB: Tryptic Soy Broth

TOH: Time of Harvest

WTA: Wall Teichoic Acid

# CHAPTER 1 GENERAL INTRODUCTION

## 1.1 *Staphylococcus aureus*

*Staphylococcus aureus* (*S. aureus*) is a Gram-positive coccus, commensal, pathogenic bacterium which causes opportunistic infections in humans and animals. It has been well known that *S. aureus* produces virulence factors, such as protein A, enterotoxins, toxic shock syndrome toxin, etc. (1).

Currently, antibiotic resistance in this species has been threatening our public health. Methicillin-resistant *S. aureus* (MRSA), carrying the *mecA* gene responsible for resistance to all beta-lactam antibiotics, is a major cause of hospital-acquired infections in hospitals worldwide (2-4). Although the combination of antibiotics (vancomycin, linezolid, daptomycin, etc.) is the general treatment for *S. aureus* infections including MRSA, the emergence and spread of the antibiotic-resistant bacteria have been globally concerned as well as other microbials (4, 5). In 2014, it was reported that at least 700,000 lives die each year due to drug resistance in microbial infections, and the number of deaths by drug resistance would reach up to ten million in 2050 if resistance was kept to current level (6). To combat antimicrobial resistance, WHO endorsed a global action plan in 2015 with five strategic objectives (7):

1. Improve awareness and understanding of antimicrobial resistance through effective communication, education, and training
2. Strengthen the knowledge and evidence base through surveillance and research
3. Reduce the incidence of infection through effective sanitation, hygiene, and infection prevention measures
4. Optimize the use of antimicrobial medicines in human and animal health
5. Develop the economic case for sustainable investment that takes account of the needs of all countries and to increase investment in new medicines, diagnostic tools,

vaccines, and other interventions

The countermeasures for antimicrobial resistance require the global actions in multiple layers and fields based on above five concepts. Thus, development of the alternatives to antibiotic-based treatment should be considered for *S. aureus* infections as described in the global action plan stated by WHO.

## 1.2 Therapeutical Application of Bacteriophages

Bacteriophage (phage) is a virus which infects bacteria. It is well known that the host bacteria are lysed by phages during their infectious process. Since Frederik W. Twort discovered phages in 1915, its therapeutic potential had been attracted until Alexander Fleming discovered the first antibiotic penicillin in 1929 because penicillin is effective to most bacteria while the spectrum of phages is limited in species by species. Due to the antibiotic-resistance in pathogenic bacteria, the clinical application of phages (phage therapy) has been reassessed (8, 9). To date, both the effectiveness and safety of phages have been demonstrated in animals including worms, mice, rats, rabbits, and humans (10-16). Therefore, the use of phages against bacterial infections is considered as one of the alternative treatments to antibiotics.

Currently, phage therapy has not been commercially available except Georgia and Russia (17, 18). Several clinical trials have been conducted as shown in Table 1.

**Table 1 The status of major clinical studies related to phage therapy.**

| Code | Indication (target) | Phase | Study period | Origin (country) |
|---|---|---|---|---|
| LBP-EC01 | Urinary-tract infection (*E. coli*) | P2/P3 | Jul. 2022 - Dec. 2025 | Locus Biosciences (US) |
| AP-SA02 | Bacteremia (*S. aureus*) | P1b/P2a | Apr. 2022 - Dec. 2023 | Armata Pharmaceuticals, Inc. (US) |
| BX005-A | Atopic dermatitis (*S. aureus*) | P1b/P2a | May. 2022 - Jun. 2023 | BiomX (Israel) |

The information in this table is taken from ClinicalTrials.gv (https://clinicaltrials.gov/) in 2022.

The therapeutical applications of phages on humans have been also conducted as compassionate uses, where some cases have been resulted in complete cures (19). While the achievement of phage therapy is sufficient enough to explain the therapeutical capability of phages, the preparation of phages for clinical use should be further improved. For instance, a clinical trial in 2015 and 2017 on a burn wound infected with *Pseudomonas aeruginosa* in hospitals in France and Belgium (known as PhagoBurn) was failed due to the unexpected decrease of phage titer in 1000-fold to 10,000-fold, which was observed after mixing several types of phages as cocktail (20). Although preliminary studies of shelf-life stability were conducted by use of two representative single phage preparations before the clinical trial, the stability study with final product should have been required. In addition, an adverse event (fever, wheezing, and shortness of breath) was observed at the therapeutic use of phages for humans in University of California, San Diego, possibly due to the unknown pyrogens (impurities) derived from the phage solution apart from endotoxin (10). Thus, the preparation of phages for therapeutic use has to be considered as one of the current concerns in phage therapy.

## 1.3 Manufacturing of Phages as Pharmaceuticals

In the treatment of *S. aureus* infections, phages have been prepared in bulk and administered to multiple patients (13). For this therapeutic use, the quality of phages is

required to be controlled under a regulatory framework of good manufacturing practices (GMP) by health authorities (e.g., Food and Drug Administration, European Medicines Agency, Pharmaceuticals and Medical Devices Agency) as well as other pharmaceuticals (21). In addition to the quality control under GMP regulation, the manufacturing process is recommended to be developed by quality-by-design (QbD) approach, which is described in guidelines by International Council for Harmonisation of Technical Requirements for Pharmaceuticals for Human Use (ICH). The goal of QbD approach is to ensure the drug quality by proper control of process parameters in the manufacturing from the development stage (22, 23). As shown in Figure 1, the concept of QbD approach is composed of below steps.

1. Identify the critical quality attributes (CQAs) of the drug based on quality target product profile (QTPP) which is defines from expectation as the drug quality (i.e., mechanism of action, efficacy, and safety as the drug).

2. Investigate the effects of process parameters on CQAs by using risk assessment and experiments at a laboratory.

3. Define the acceptable ranges of process parameters (called as “design space”) and implement in the manufacturing as control strategy for quality assurance.

As one of the general concepts in QbD approach, the application of statistical tools is recommended to investigate the relationship between CQAs and process parameters such as multivariate studies. Since proposed in 2010s, QbD approach has been applied into process development for the drug manufacturing in a wide variety of modalities (small molecules, antibody, cell products, virus vectors for gene therapy, etc.) (23-26). QTPP and CQAs for phages have been partially discussed and following factors are suggested as CQAs: identity, titer, general purity, endotoxin, contamination by toxic bacterial proteins, and nucleic acid contaminants (22). However, the relationships between process

parameters and each CQA have not been fully investigated. Therefore, process development for the manufacturing of phages should be conducted to understand the process parameters impacted on CQAs based on the concept of QbD approach for the quality control of the products.

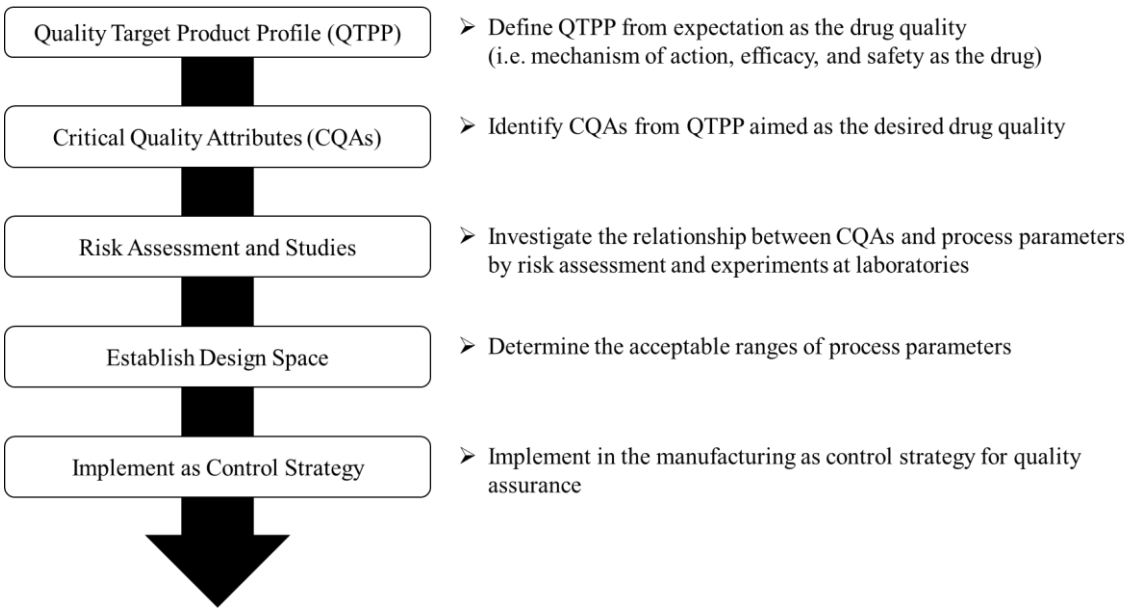


**Figure 1 The scheme of QbD approach.**

## 1.4 Scope of This Study

In order to realize the phage therapy against *S. aureus* infections, a series of studies are conducted under the concept of QbD approach to establish the manufacturing of *S. aureus* phages. To understand the nature of *S. aureus* phages toward quality control in the manufacturing, *S. aureus* phage ΦSA012 was characterized as described in Chapter 2. To investigate the optimal condition for the manufacturing, the propagation processes of *S. aureus* phages S13′ and S25-3 were investigated as described in Chapter 3. Finally, the conclusions of this study are described in Chapter 4.

# CHAPTER 2 CHARACTERIZATION OF *S. aureus* PHAGE ΦSA012

## 2.1 Introduction

In order to understand the nature of *S. aureus* phages for the manufacturing, *S. aureus* phage ΦSA012 was studied as described in this chapter. ΦSA012, which was isolated from wastewater, showed wide host range and highly lytic capability against *S. aureus* strains from bovine mastitis (27). Thus, ΦSA012 is considered as one of promising candidates for phage therapy against *S. aureus*, and ΦSA012 was chosen to be characterized in this chapter. To understand the genomic character of ΦSA012, whole genome analysis of ΦSA012 was conducted. The mechanism of infections against *S. aureus* in ΦSA012 has been also investigated for further characterization of ΦSA012.

## 2.2 Materials and Methods

### 2.2.1 Bacterial strains, phages, plasmids, and culture conditions

Bacterial strains, phages, and plasmids are listed in Table 2. *S. aureus* strain RN4220 was used for gene manipulations (28). *S. aureus* phage ΦSA012 was isolated from sewage in a previous study (27). *S. aureus* strain SA003, which was isolated from raw milk samples from a mastitic cow, was used for propagation and enumeration of *S. aureus* phages. ΦSA012 and SA003 were deposited in NITE Biological Resource Center (Kisarazu, Japan) under accession numbers NBRC110649 and NBRC110650, respectively. *S. aureus* strain RN4220 was kindly supplied by Prof. Motoyuki Sugai (Hiroshima University Graduate School of Biomedical & Health Sciences, Hiroshima, Japan) with the permission of Prof. Richard P. Novick (Skirball Institute of Biomolecular Medicine, New York, NY, USA) and used for gene manipulation (28). *Escherichia coli* (*E. coli*) strain JM109 and Rosetta-gami™ 2 (DE), used for plasmid construction and expression of proteins, were purchased from Takara Bio (Otsu, Japan) and Novagen/Merck Millipore (Darmstadt, Germany), respectively. Shuttle vectors pNL9164

and pLI50 were purchased from Sigma-Aldrich (St. Louis, MO, USA) and Addgene (Cambridge, MA, USA), respectively. The shuttle vector pKOR1 was kindly supplied by Dr. Taeok Bae (Indiana University School of Medicine-Northwest, Indianapolis, IN, USA). Expression vector pET29a was purchased from Novagen/Merck Millipore (Darmstadt, Germany). All *S. aureus* and *E. coli* strains were grown at 37°C in Luria-Bertani (LB) medium overnight, unless otherwise stated.

**Table 2 Bacterial strains, phages, and plasmids.**

| Bacterial strain, phage or plasmid | Relevant features | Reference |
|---|---|---|
| *S. aureus* strains | | |
| SA003 | Host strain, isolated from bovine mastitis, lack of *tarM* | (27) |
| SA003R11 | ΦSA012-resistant derivative | (29) |
| SA003R20 | ΦSA012-resistant derivative | (29) |
| RN4220 | Restriction deficient, transformable strain | (28) |
| RN4220Δ*tarM* | The in-frame deletion mutant of *tarM* in RN4220 | (29) |
| RN4220Δ*tarM*::pLIP3_tarM | Complemented RN4220Δ*tarM* strain of *tarM* with the plasmid pLIP3_tarM | This study |
| *E. coli* strains | | |
| JM109 | Used for plasmid constructions | Takara Bio |
| Rossetta-gami™ 2 (DE) | Used for expression of recombinant proteins | Novagen |
| Phages | | |
| ΦSA012 | *S. aureus* lytic phage | (27) |
| ΦSA012M1 | Spontaneous mutant phage | (29) |
| ΦSA012M2 | Spontaneous mutant phage | (29) |
| ΦSA012M11 | Spontaneous mutant phage | (29) |
| ΦSA012M20 | Spontaneous mutant phage | (29) |
| ΦSA012M38 | Spontaneous mutant phage | (29) |
| ΦSA012TM103 | Harboring three mutations in *orf103* | This study |
| Plasmids | | |
| pKOR1 | *E. coli*/*S. aureus* shuttle vector, temperature-sensitive | (30) |
| pLI50 | *E. coli*/*S. aureus* shuttle vector | Addgene |
| pLIP3_tarM | *tarM* expression plasmid driven by pLI50 | This study |
| pNL9164 | *E. coli*/*S. aureus* shuttle vector | Sigma |
| pET-29a | Expression vector for production of recombinant proteins | Novagen |

### 2.2.2 Phage preparation

All phages were propagated by the plate-lysate method (31). Briefly, 100 µl of phage lysate (> $10^5$ plaque-forming units (PFU)/ml) was mixed with 100 µl of overnight bacterial culture in 3 ml of 0.5% top agar, plated on LB-agar, and incubated at 37°C overnight. After 5 ml of salt magnesium (SM) buffer (100 mM NaCl, 8 mM $MgSO_4$, 50 mM Tris-HCl [pH 7.5], 0.01% gelatin) was added to the plate and the over-layer was scraped off to extract phages, the supernatant was collected by centrifugation (5,000 ×*g*, 15 min, 4°C) and purified by PEG sedimentation (10% PEG-6000, 4% NaCl) and CsCl density gradient centrifugation (31). Each phage culture was titered and stored at 4°C until use.

### 2.2.3 Extraction and analysis of phage genomic DNA

Genomic DNA of ΦSA012 was extracted from purified phages using a phage DNA isolation kit (Norgen Biotek Corp, Thorold, ON, Canada). Whole-genome sequencing was performed on a Genome Sequencer FLX+System (Roche, Basel, Switzerland). Sequencing results were assembled and aligned using GS De Novo Assembler v2.8 (Roche, Basel, Switzerland) and Tablet (The James Hutton Plant Bioinformatics Group, Invergowrie, Scotland), respectively. Open reading frames (ORFs) were predicted with myRAST (http://blog.theseed.org/servers/presentations/t1/running-a-job-with-the-desktop-rast.html). Nucleotide and amino-acid sequences were scanned for homologs using BLAST (32). Phage-encoded tRNA genes were identified using Aragorn and the tRNA Scan SE software, ver. 1.21 (33, 34). The complete genome of ΦSA012 has been deposited in the GenBank database under accession number AB903967.

### 2.2.4 Molecular cloning in *S. aureus*

The primers used in this study are shown in Table 3. Deletion of *tarM* in *S. aureus* RN4220 was performed using shuttle vector pKOR1 as described before (30). A DNA

fragment for allelic exchange was prepared by “splicing by overlap extension PCR”, digested with EagI and EcoRV, and inserted into pKOR1 (New England Biolabs, Ipswich, MA, USA). The resultant plasmid was constructed in *E. coli* JM109 and electroporated into *S. aureus* RN4220 (35). An *S. aureus* strain in which the plasmid had integrated into the genome was selected at 43°C in the presence of chloramphenicol (10 μg/ml). Subsequently, the plasmid was excised and cured by culturing the strain in brain-heart infusion (BHI) medium at 30°C or 43°C. To screen for plasmid-free strains, colonies were replica-plated onto tryptic soy broth (TSB) agar with or without chloramphenicol (10 μg/ml). Anhydrotetoracycline (1 μg/ml) was used for counterselection. Gene deletion was confirmed by PCR with the appropriate primer set (Table 3). For complementation of *tarM*, the plasmid pLIP3_tarM for ectopic expression of *tarM* was constructed by integrating the P3 promoter, which is constitutive in *S. aureus*, and the *tarM* gene in the shuttle vector pLI50 (36, 37). DNA fragments corresponding to the P3 promoter and *tarM* were amplified from genomic DNA of RN4220 and inserted into pLI50. The plasmid pLIP3_tarM was constructed in *E. coli* JM109, and then electroporated into *S. aureus* RN4220Δ*tarM* (35).

**Table 3 The list of primers for molecular cloning in *S. aureus*.**

| Primer | Direction | Sequence (5'->3')[a] | Description |
|---|---|---|---|
| PKOR1 insert_c_F | Forward | CACAGGAAACAGCTATGACATAG | Insert check in pKOR1 |
| PKOR1 insert_c_R | Reverse | CAGGTACATCATTCTGTTTGTG | |
| tarM_A_Eag1 | Forward | AAA**CGGCCG**TGAAATTGAAGAGAGTAAAGGTATTTC | |
| tarM_B | Reverse | TTTTGGAAAACTCCCTGGTCC | SOEing PCR for deletion of *tarM* |
| tarM_C | Forward | GGACCAGGGAGTTTTCCAAAAGGTCAAGGGTTAAGTATGATAGAAG | |
| tarM_D_EcoRV | Reverse | AAA**GATATC**AGTAGTTACAGCTGGAAGAAA | |
| tarM_Fw | Forward | AATGGATCGAAGAACGAAAATGT | Check for deletion of *tarM* |
| tarM_Rv | Reverse | ACGCCTTATGTTAATGTTTTTTATATTTG | |
| pLI50-insertcheck-fw | Forward | TAATACCGCGCCACATAGCAGAAC | Insert check in pLI50 or pLIP3 |
| pLI50-insertcheck-rv | Reverse | TAGCTCACGCTATGCCGACATTC | |
| P1075_EcoR1 | Forward | AAA**GAATTC**GAGTGGTATAAGTGGTTTTTCG | For DNA fragment of P3 promoter |
| P697_Kpn1 | Reverse | AAA**GGTACC**TTCACCTCTGTTCTTACGACCTC | |
| TarM_e_p3_Fw | Forward | AAA**CCCGGG**GAGGTAAAGGAATAATTATAATGAAAAAAA | Complementation of *tarM* |
| TarM_e_Rv | Reverse | AAA**GTCGAC**TTAGCTATTGAAAAGATTTAACCATTTTTC | |
| ORF103M-F | Forward | CCC**AAGCTT**GGGGGGTTGATTGACCCCTCTTT | Introduction of mutations into a recombinant phage |
| ORF103M-R | Reverse | CCC**AAGCTT**GGGCCCTAGCTCCTTGTCATACCC | |
| ORF103b-F | Forward | TGAATCCACAACTCAATATGCAAC | Check of mutations in a recombinant phage |
| ORF103c-F | Forward | TCATCTAGTAAAGGTAATGGTGC | |
| ORF103r-F | Forward | GGGAATTC**CATATG**GCATTTAACTACACGCCTC | The expression of ORF103 |
| ORF103r-R | Reverse | CCG**CTCGAG**TCCTCTATTAATTCCCATAATATTGTATACC | |
| ORF105r-F | Forward | GGGAATTC**CATATG**GCATTTAACTACACGCCTC | The expression of ORF103 |
| ORF105r-R | Reverse | CCG**CTCGAG**TCCTCTATTAATTCCCATAATATTGTATACC | |
| pET29a_Insert-c_F | Forward | CATGAGCCCGAAGTGGCGAGCCCGATCTTC | Insert check in pET29a |
| pET29a_Insert-c_R | Reverse | CGCTGCGCGTAACCACCACACCCGCCGCGC | |

[a] Bold and underlined indicate restriction sites.

### 2.2.5 Isolation of mutant phages from co-culture experiments

In order to isolate ΦSA012-resistant derivatives and mutant phages, SA003 and ΦSA012 were co-cultured (29). SA003 was inoculated into 4.5 ml of LB medium and cultured until early exponential phase (optical density at 660 nm ($OD_{660}$) = 0.1) in a TVS062CA compact rocking incubator (Advantec, Tokyo, Japan). Approximately 4.5 × $10^8$ PFU of ΦSA012 was added at MOI = 1 and cultured at 37°C with shaking at 40 rpm. After 2-10 days, bacteria/phage mixed cultures were collected. Forty-five microliters of bacteria/phage mixed culture was transferred into 4.5 ml of fresh LB medium (1:100 dilution) and cultured under the same conditions. After 2-10 days, the bacteria/phage mixed culture was collected, and a 1:100 dilution was performed again.

For isolation of ΦSA012-resistant derivatives and mutant phages, 1.5 ml of mixed culture collected from co-culture was separated by centrifugation (9,730 ×*g*, 5 min, 4°C) at each passage step. After washing four times with phosphate-buffered saline (PBS) to remove free phages, the pellet was resuspended in PBS and spread onto LB plates; one colony was picked as a ΦSA012-resistant derivative after overnight incubation. Supernatant from the co-culture was used for a plaque assay with SA003. After overnight incubation, one plaque was also picked as a mutant phage.

This procedure was repeated continuously until the 38$^{th}$ passage. ΦSA012-resistant derivatives and mutant phages were defined as SA003R1-SA003R38 and ΦSA012M1-ΦSA012M38, respectively. Each number in the name of ΦSA012-resistant derivatives and mutant phages represents the number of passages in co-culture (e.g., SA003R11 means ‘phage-resistant derivative isolated from the co-culture at the 11$^{th}$ passage’, and ΦSA012M20 means ‘mutant phage isolated from the co-culture at the 20$^{th}$ passage’). In order to identify the mutation points, genomic analysis of five mutant phages (ΦSA012M1, ΦSA012M2, ΦSA012M11, ΦSA012M20, and ΦSA012M38) were conducted in aforementioned method.

### 2.2.6 Generation of recombinant phages harboring mutations in *orf103*

The scheme for generation and isolation of recombinant phages harboring mutations in *orf103* is shown in Figure 2. In order to construct the plasmid harboring three mutations in ORF103, a DNA fragment was amplified from genomic DNA of ΦSA012M20 by PCR using primers ORF103M-F and ORF103M-R. This PCR fragment contained the nucleotide sequence between 200 bp upstream and 110 bp downstream of *orf103*. The recombinant fragment was digested with HindIII (Takara Bio) and inserted into the shuttle vector pNL9164 (38). The plasmid was constructed and cloned in *E. coli* JM109. The constructed plasmid (named pNL9164::TM*orf103*) was then electroporated into *S. aureus* strain RN4220 (35).

A recombinant phage ΦSA012 harboring three mutations in *orf103* (ΦSA012TM103) was generated by the following procedure. Transformed RN4220 harboring pNL9164::TM*orf103* was grown to early exponential phase ($OD_{660}$ = 0.1, $10^8$ colony-forming units (CFU)/ml) at 32°C with shaking at 120 rpm in 10 ml of LB medium. Then, $10^6$ PFU/ml of ΦSA012 was added at multiplicity of infection (MOI) = 0.01. In phage infection, homologous recombination between phage DNA and the plasmid in transformed RN4220 harboring ORF103 of ΦSA012M20 might happen with low frequency. After overnight incubation at 32°C with shaking, the supernatant was collected by centrifugation (6,230 ×*g*, 10 min, 4°C) and plated by the plaque assay for isolation of ΦSA012TM103. Briefly, 500 µl of phage lysate and 250 µl of overnight culture of phage-resistant derivative SA003R11 (susceptible to ΦSA012M20, but not ΦSA012) were added to 6 ml of 0.5% top agar and poured onto LB-agar plates. After incubation overnight at 37°C, single plaques were picked and resuspended in 100 µl of SM buffer. These suspensions were purified by two rounds of the plaque assay with SA003R11. Mutations in *orf103* of ΦSA012TM103 were identified by Sanger sequencing using primers ORF103b-F and ORF103c-F.

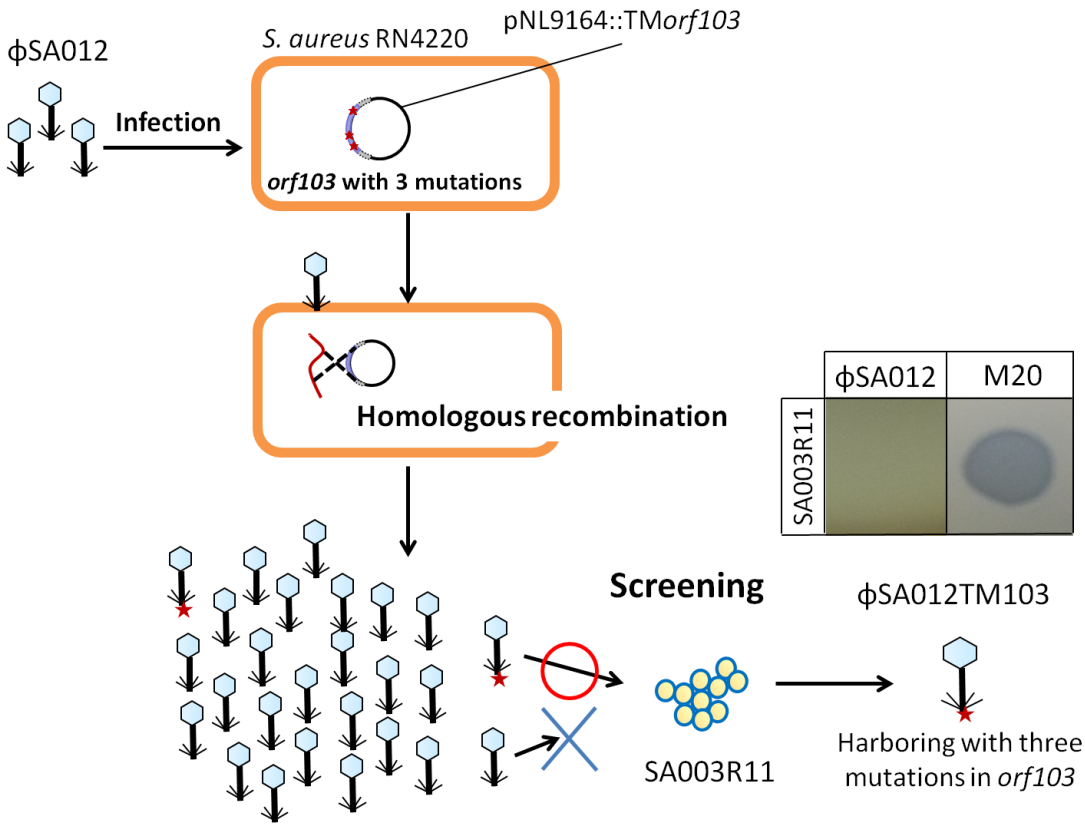


**Figure 2 Scheme of generation of a recombinant phage ΦSA012TM103.**

Three mutations found in *orf103* among mutant phages were introduced into wild type ΦSA012 by homologous recombination between phage DNA and plasmid pNL9164::TM*orf103* in *S. aureus* RN4220. ΦSA012TM103 was screened from the population of phages composed of a large number of wild type and very few of recombinant phages by the plaque assay with a ΦSA012-resistant derivative SA003R11 susceptible to mutant phages harboring three mutations in *orf103*, but not to ΦSA012. It was assumed that only a recombinant phage can produce a plaque in SA003R11.

### 2.2.7 Protein expression and purification

C-terminally His-tagged recombinant ORF103 and ORF105 were expressed in *E. coli* Rosetta-gami™ 2 (DE) from vector pET-29a and purified by immobilized metal ion affinity chromatography (IMAC). To construct plasmids for expression of ORF103 and ORF105, DNA fragments were amplified by PCR with the appropriate primer sets (Table 3). Recombinant fragments for protein expression were digested with NdeI and XhoI (New England Biolabs), and then inserted into pET-29a. The plasmids were constructed and cloned in *E. coli* JM109, and then electroporated into *E. coli* Rossetta-gami™ 2 (DE).

To produce ORF103 and ORF105 proteins, expression was induced by addition of 1 mM (isopropyl β-D-1-thiogalactopyranoside) when the culture reached at optical density at 600 nm ($OD_{600}$) = 0.5. After incubation at 28°C with shaking at 160 rpm overnight, the cells were collected by centrifugation (6,230 ×*g*, 10 min, 4°C), resuspended in phosphate buffer (20 mM phosphate [pH 7.4], 0.5 M NaCl), and disrupted by sonication for 40 min in a VP60-S (TAITEC, Koshigaya, Japan). Target proteins were purified using a HisTrap HP (GE healthcare Life sciences, Buckinghamshire, UK). After His-tagged proteins were eluted from the Ni-column with elution buffer (40-500 mM imidazole in phosphate buffer), the imidazole was removed by dialysis against phosphate buffer.

### 2.2.8 Preparation of antibodies

Polyclonal rabbit antibodies against recombinant proteins ORF103 and ORF105 were generated by Japan Bio Serum (Hiroshima, Japan). Briefly, rabbits were immunized with 0.3 mg of the protein once every two weeks for eight weeks; in total, 1.5 mg of protein was used. After blood was collected in week 10, anti-ORF103 serum was purified on a protein A column and stored at -20°C until use.

### 2.2.9 Immunoelectoron microscopy

Immunoelectron microscopy was conducted as described previously (39). Fresh purified phage sample ($10^{10}$ PFU/ml) was mixed with purified anti-ORF103 antibody diluted in SM buffer (1:100) and incubated at room temperature for 30 min. The samples were loaded onto ester-carbon-coated copper grids (EMJapan, Tokyo, Japan). The copper grids were washed twice with SM buffer and incubated with 12 nm Colloidal Gold-AffiniPure Goat Anti-Rabbit IgG (H+L) (Jackson ImmunoResearch Laboratories, West Grove, PA, USA) in PBS buffer (1:50) at 37°C for 30 min. After washing with SM buffer and Milli-Q water twice each, the grids were stained with 2% uranyl acetate and observed on a JEM-1400Plus (JEOL, Akishima, Japan).

### 2.2.10 Spot test and efficiency of plating (EOP) with antibodies

The infectivity of phages was evaluated as previously described (27). Briefly, 2 µl of serial diluted phage lysate ($10^{7}$-$10^{10}$ PFU/ml) was dropped onto an LB plate overlaid with *S. aureus* strains mixed with 0.5% top agar, and then incubated overnight to assess plaque formation (i.e., turbidity of plaque).

EOP of phages on *S. aureus* strains with the antibodies was measured by the plaque assay with phage lysate adjusted with SA003. For assay with an antibody to evaluate the role of ORF103 or ORF105 in infection, 10 µl of anti-ORF103 or anti-ORF105 serum was added into 100 µl of phage lysate. After incubation for 1 h at room temperature, the number of infectious phages enumerated by the plaque assay with SA003. Serum collected from a rabbit before immunization (pre-immunized serum) was used as a control.

### 2.2.11 Adsorption assay

Adsorption efficiency of phages in *S. aureus* strains was measured by titrating free phages present in the supernatant after defined periods of cell/phage contact. *S. aureus* cells were prepared by 10% inoculation of overnight culture into 4.5 ml of LB medium;

the culture was then incubated at 37°C with shaking at 120 rpm until $OD_{660}$ = 1.0 (~$10^9$ CFU/ml). Then, phage lysate ($10^7$ PFU/ml) was added to the bacterial culture. After infection at 37°C with shaking at 120 rpm, free phages were collected by centrifugation (9,730 ×*g*, 1 min) at defined times and titered using SA003. For longer incubation, 50 μg/ml of chloramphenicol or erythromycin was added, and cells were equilibrated for 10 min at 37°C before infection to inhibit cell growth and phage development during incubation with phages (40). Adsorption efficiency was calculated by dividing the number of adsorbed phages by the initial number of phages.

### 2.2.12 Statistical analysis

Two-tailed Student's *t* test was used to determine statistical significance.

## 2.3 Results

### 2.3.1 Genomic analysis of ΦSA012

Whole-genome sequencing of ΦSA012 revealed that ΦSA012 belongs to the genus *Kayvirus* (previously named as *Twortlikevirus*) and its genome is 142,094 bp in length and contains 207 ORFs (APPENDIX). Three tRNA genes (Met-tRNA: 8,180-8,109 bp; Asp-tRNA: 30,496-30,423 bp; Phe-tRNA: 30,416-30,344 bp) are encoded in the ΦSA012 genome. It was also revealed that ΦSA012 shares high similarities at the genomic level with phage K (97.00% of identity), phage ISP (96.97% of identity) and phage S25-3 (98.60% of identity).

### 2.3.2 Characterization of mutant phages derived from ΦSA012

From the results of spot test with ΦSA012-resistant derivatives and mutant phages, it was confirmed that phenotypic changes had been continuously caused by antagonistic co-evolution (Figure 3) (29). For instance, ΦSA012M2 formed clear plaques on SA003R2, but the subsequently arising bacterial strain SA003R11 developed resistance

to ΦSA012M2, as determined by faint plaque formation. By contrast, the later-generation phage ΦSA012M11 formed clearer plaques on SA003R11 than ΦSA012M2. Similar phenomena were observed in subsequent plaques. In addition, the latest isolates SA003R38 and ΦSA012M38 possessed the highest and widest range of resistance and infectivity, respectively: no phage formed plaques on SA003R38, whereas ΦSA012M38 formed the clearest plaques on SA003R11, SA003R17, and SA003R20, although they were still turbid. As linked to the changes of phenotypic changes, genetic mutations in ΦSA012-resistant derivatives were founded among several genes, which inhibited the phage adsorption (41). Therefore, it is likely that these mutant phages possess the mutations in the genes related to their infectivity, too.

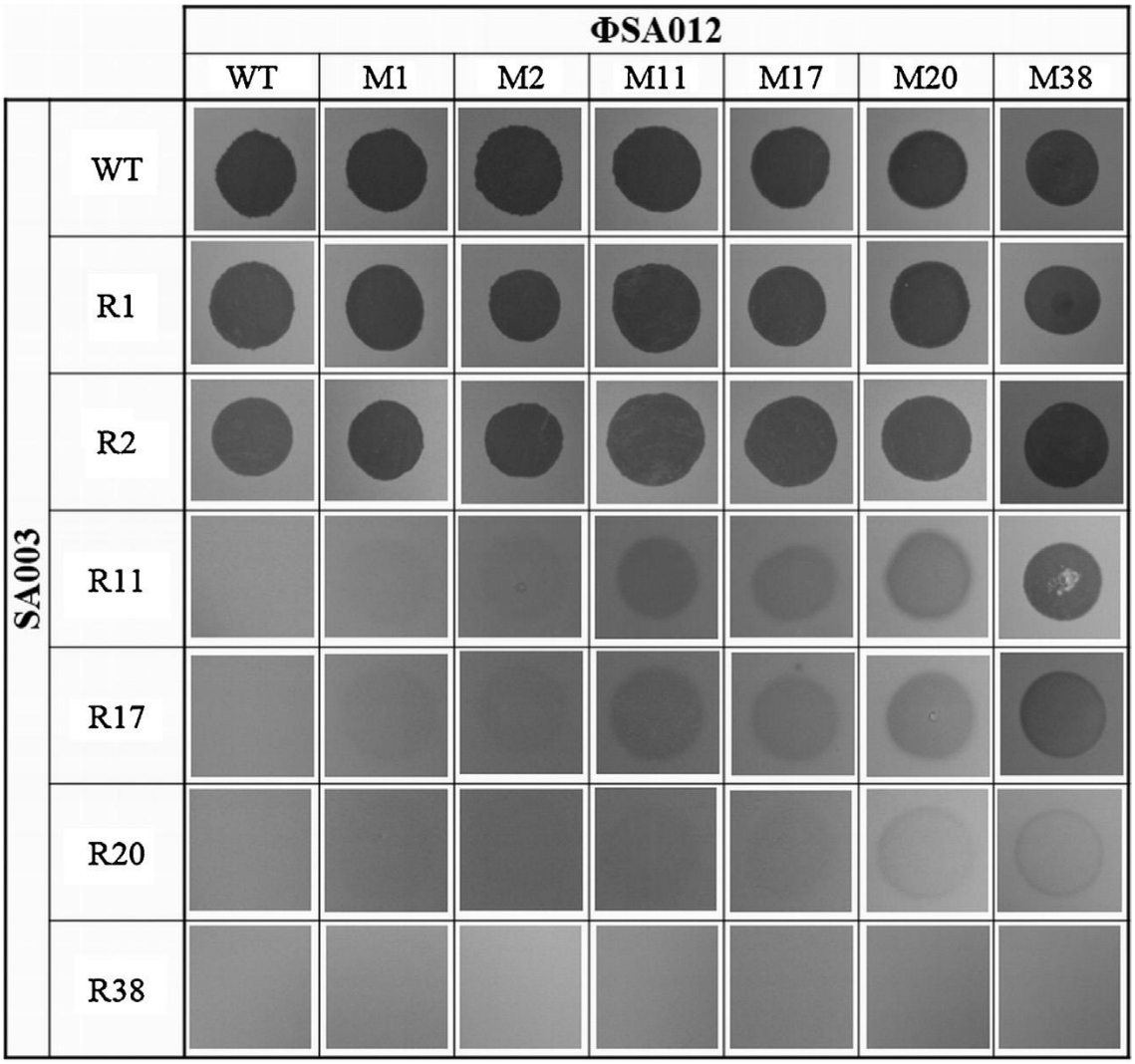


**Figure 3 Spot test among isolates from co-culture.**

The vertical dimension depicts phenotypic changes of SA003 as serial transfer proceeded (from top to bottom), whereas the horizontal dimension depicts the phenotypic changes of the phage (from left to right) (29).

In order to find the candidate genes responsible for host recognition, all mutations in five mutant phages (ΦSA012M1, ΦSA012M2, ΦSA012M11, ΦSA012M20, and ΦSA012M38) isolated from co-cultures were identified by whole-genome sequencing (Table 4). Mutations were found in six ORFs (*orf33*, *orf58*, *orf79*, *orf99*, *orf103*, and *orf133*) and terminally redundant regions, located in both ends of the genome, which contain several thousand base pairs and nonpermuted direct terminal repeats.

Deletion of 1-1,045 bp (containing *orf1-orf3*) and 141,673-142,094 bp (containing *orf207*) was detected in five mutant phages (Table 3). In SPO1, these terminally redundant regions contain the host-takeover module (42). In phages under the genus *Kayvirus*, it has also been suggested that some or all genes located in these regions play a role in host takeover, by analogy to the corresponding regions of SPO1 (43). Insertion of one nucleotide in *orf58* caused a frame shift and generated a premature stop codon, leading to partial deletion of the gene product (aa 85-108). *orf58* encodes a protein homologous to membrane protein MbpC of phage A5W; it is predicted to play a role in attachment of the complex of replicating phage DNA to a cell membrane, analogous to membrane protein p16.7 of *Bacillus* phage φ29 (43, 44). Although substitution of amino acids in *orf33* was only observed in ΦSA012M2, it did not accumulate among later mutant phages. Other ORFs in which mutations were observed (*orf79*, *orf99*, *orf103*, and *orf133*) encode putative tail proteins. *orf79* is predicted to encode the tail sheath protein, and has homologs in a number of phages. The functions of *orf99* and *orf103*, predicted as tail morphogenic proteins, remain unknown. Due to the presence of immunoglobulin (Ig)-like domain conserved among hundreds of phages, *orf133* is predicted to encode a tail protein that plays an accessory role by interacting weakly with carbohydrates on the bacterial surface (43, 45, 46).

**Table 4 Distribution of mutation points in mutant and triple-mutated phage.**

| Position (bp)[a] | 1 - 1045 | 16908 | 33020 (A)[b] 33021 | 50380 | 71775 | 71909 | 78605 | 79071 | 79167 | 107746 | 141673 -142094 |
|---|---|---|---|---|---|---|---|---|---|---|---|
| **ΦSA012** | *orf1/2/3* | *orf33* | *orf58* | *orf79* | *orf99* | | *orf103* | | | *orf133* | *orf207* |
| **Predicted function** | **Terminally redundant region** | **Un-known** | **Hypothetical membrane protein** | **Tail sheath protein** | **Tail morphogenetic protein** | | **Virion component (a part of tail fiber?)** | | | **Tail morphogenetic protein (Ig-like)** | **Terminally redundant region** |
| ΦSA012 (wild type) | +[c] | GAA<br>E | ACA TCT TAC<br>T S Y | TTC<br>F | AAT<br>N | TCT<br>S | AAT<br>N | GGT<br>G | ACA<br>T | GTA<br>V | +[c] |
| ΦSA012M1 | +[c] | GAA<br>E | ACA TCT TAC<br>T S Y | TTC<br>F | AAT<br>N | TCT<br>S | AAT<br>N | GGT<br>G | A**G**A<br>R | GTA<br>V | +[c] |
| ΦSA012M2 | +[c] | **A**AA<br>K | ACA TCT TAC<br>T S Y | TTC<br>F | AAT<br>N | TCT<br>S | **G**AT<br>D | GGT<br>G | A**G**A<br>R | GTA<br>V | +[c] |
| ΦSA012M11 | Deleted | GAA<br>E | ACA TCT TAC<br>T S Y | TT**A**<br>L | AAT<br>N | TCT<br>S | **G**AT<br>D | GGT<br>G | A**G**A<br>R | GTA<br>V | Deleted |
| ΦSA012M20 | Deleted | GAA<br>E | A**A**C ATC TTA<br>N I L | TT**A**<br>L | AA**G**<br>K | TCT<br>S | **G**AT<br>D | G**A**T<br>D | A**G**A<br>R | GTA<br>V | Deleted |
| ΦSA012M38 | Deleted | GAA<br>E | A**A**C ATC TTA<br>N I L | TT**A**<br>L | AA**G**<br>K | T**A**T<br>Y | **G**AT<br>D | G**A**T<br>D | A**G**A<br>R | **T**TA<br>L | Deleted |

[a] Positions of all mutations are indicated from the genome of ΦSA012. Gray boxes represent mutations in amino acids.

[b] Insertion of adenine (A) was discovered between 33020 bp (adenine) and 33021 bp (cytosine), resulting in a premature stop codon and partial deletion of the product (aa 85-108).

[c] The presence of the region is designated by a '+'.

Given that the largest number of mutations accumulated in *orf103*, it was hypothesized that *orf103* plays a crucial role in determining infectivity. Due to the selection pressures imposed by phage-bacterium co-evolution, phage RBPs are among the most diverse genes (47). It is worth mentioning that a carbohydrate-binding domain (1,4-β-glucanase CenC from *Cellulomonas fimi*) was identified in the central position of ORF103 (aa 221-337) by InterPro 56.0, and one of the three mutations was located within this domain (48, 49). This observation implied that ORF103 encodes a possible RBP that binds to sugar components in wall teichoic acid (WTA) on the cell surface. Thus, *orf103* was mainly focused on as one of the host determinant genes.

### 2.3.3 Comparisons of structural proteins around *orf103*

Comparisons of structural proteins (from capsid to helicase) among phages in the genus *Kayvirus* (ΦSA012, K, and ISP) and related species (SPO1 and ΦEF24C) revealed that the region from ORF103 to ORF105 is unique to *S. aureus* phages (ΦSA012, K, and ISP) at the protein level (Figure 4). The basic structural components, such as the capsid (ORF72 in ΦSA012), tail sheath (ORF79 in ΦSA012), and tape major protein (ORF89 in ΦSA012), as well as a helicase involved in DNA replication (ORF106 in ΦSA012), share higher degrees of similarity, probably due to functional similarities between the respective proteins. ORF101 in ΦSA012, predicted to be an adsorption-associated tail protein facilitating infection of Gram-positive bacteria by digesting sialic acid residues in their slime or capsules due to the presence of a putative conserved neuraminidase/sialidase domain, was also conserved among related phages (43, 50).

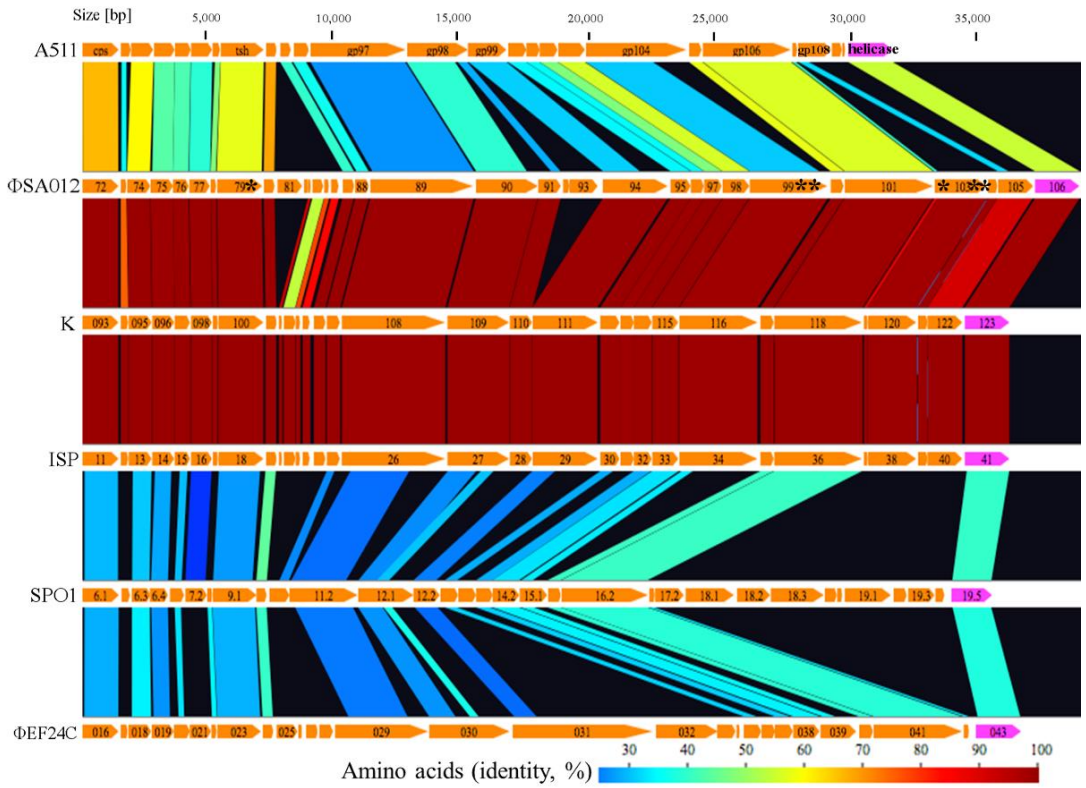


**Figure 4 Comparisons of main structural proteins among *Twortlikevirus* and related phages.**

Host bacteria of each phage are as follows: A511, *Listeria monocytogenes*; ΦSA012, K, and ISP, *Staphylococcus aureus*; SPO1, *Bacillus subtilis*; ΦEF24C, *Enterococcus faecalis*. Asterisks (*) represent the locations of mutations. Gp108 in A511 is an RBP (51). This figure was generated using GenomeMatcher (52).

### 2.3.4 Infectivity of recombinant phage harboring three mutations in *orf103*

The results of the spot test revealed that the infectivity of recombinant phage ΦSA012TM103 and mutant phage ΦSA012M20 differed from that of the wild-type phage ΦSA012 (Figure 5). All phages (ΦSA012, ΦSA012TM103, and ΦSA012M20) could produce plaques in *S. aureus* SA003. In RN4220, however, ΦSA012TM103 produced very turbid plaques, whereas ΦSA012M20 could not produce plaques, indicating that the three mutations in *orf103* inhibited infection in RN4220. Because ORF103 is likely to bind the WTA polymer due to the existence of a carbohydrate-binding domain in ORF103, the genes related to WTA synthesis was compared between SA003 and RN4220. It was found that SA003 lacked the gene *tarM*, whose product is responsible for glycosylation of α-*N*-acetylglucosamine (GlcNAc) of WTAs, whereas RN4220 had this gene (53). To investigate the importance of α-GlcNAcylation of WTAs, *tarM* was knocked out in RN4220. Deletion of *tarM* made RN4220 susceptible to ΦSA012TM103 and ΦSA012M20 harboring mutated ORF103. Thus, α-GlcNAcylation of WTAs mediated by TarM inhibited infection of ΦSA012TM103 and ΦSA012M20, but not ΦSA012. Complementation of *tarM* in the deletion mutant restored the infectivity of phages, indicating that the role of ORF103 is related to α-GlcNAc on WTAs.

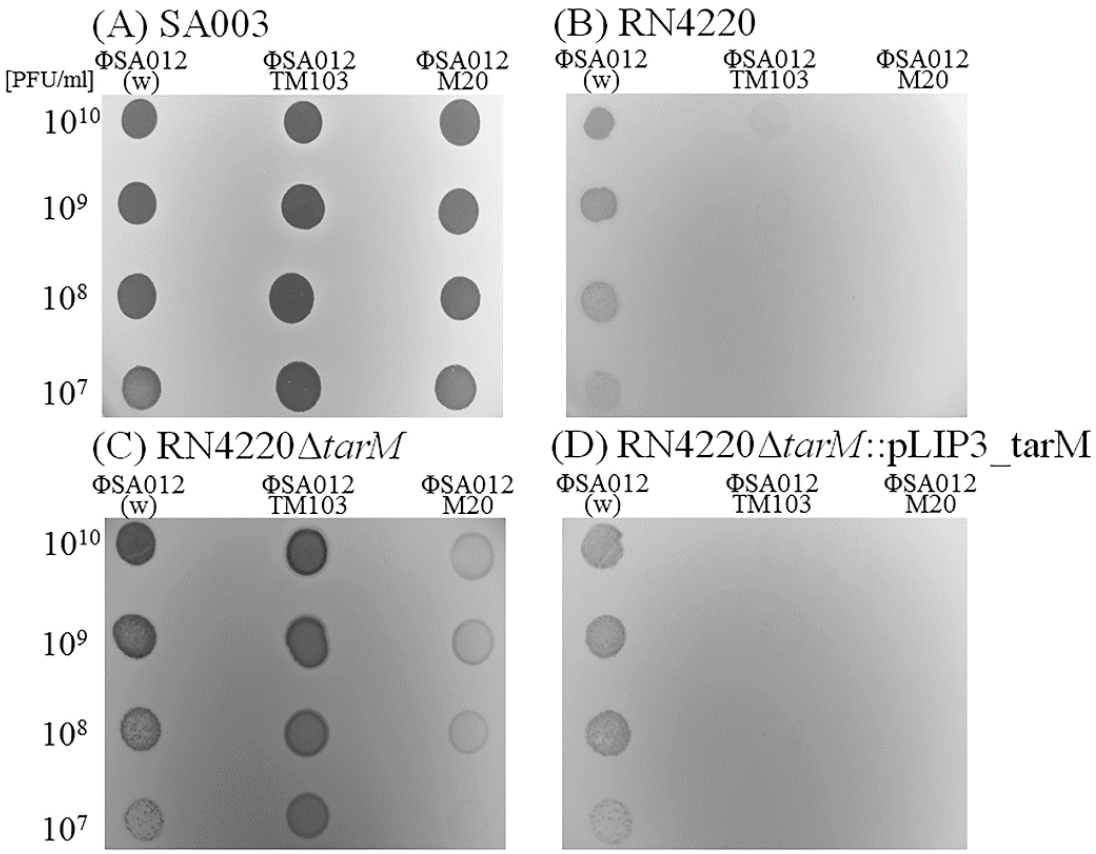


**Figure 5 Spot test of phages on *S. aureus* strains.**

Two microliters of concentrated phage lysate ($10^7$ - $10^{10}$ PFU/ml) was dropped onto an LB plate overlaid with *S. aureus* strains; (A) SA003(Δ*tarM*), (B) RN4220, (C) RN4220Δ*tarM*, and (D) RN4220Δ*tarM*::pLIP3_tarM.

The behaviors of *S. aureus* strains in adsorption assays corresponded with the results of spot tests (Figure 5 and Figure 6). In SA003, all phages (ΦSA012, ΦSA012TM103, and ΦSA012M20) had the ability to adsorb to SA003, although the adsorption efficiency of ΦSA012TM103 was lower than those of ΦSA012 and ΦSA012M20. In RN4220, on the other hand, ΦSA012TM103 and ΦSA012M20 had lower adsorption efficiencies than ΦSA012. Thus, mutations in *orf103* changed adsorption efficiency, indicating that ORF103 is involved in adsorption. Deletion of *tarM* in RN4220 enhanced adsorption efficiency of ORF103-mutated phages ΦSA012TM103 and ΦSA012M20, but did not affect adsorption of ΦSA012. Complementation of *tarM* confirmed that α-GlcNAc of WTA inhibited adsorption of ΦSA012TM103 and ΦSA012M20, but not ΦSA012.

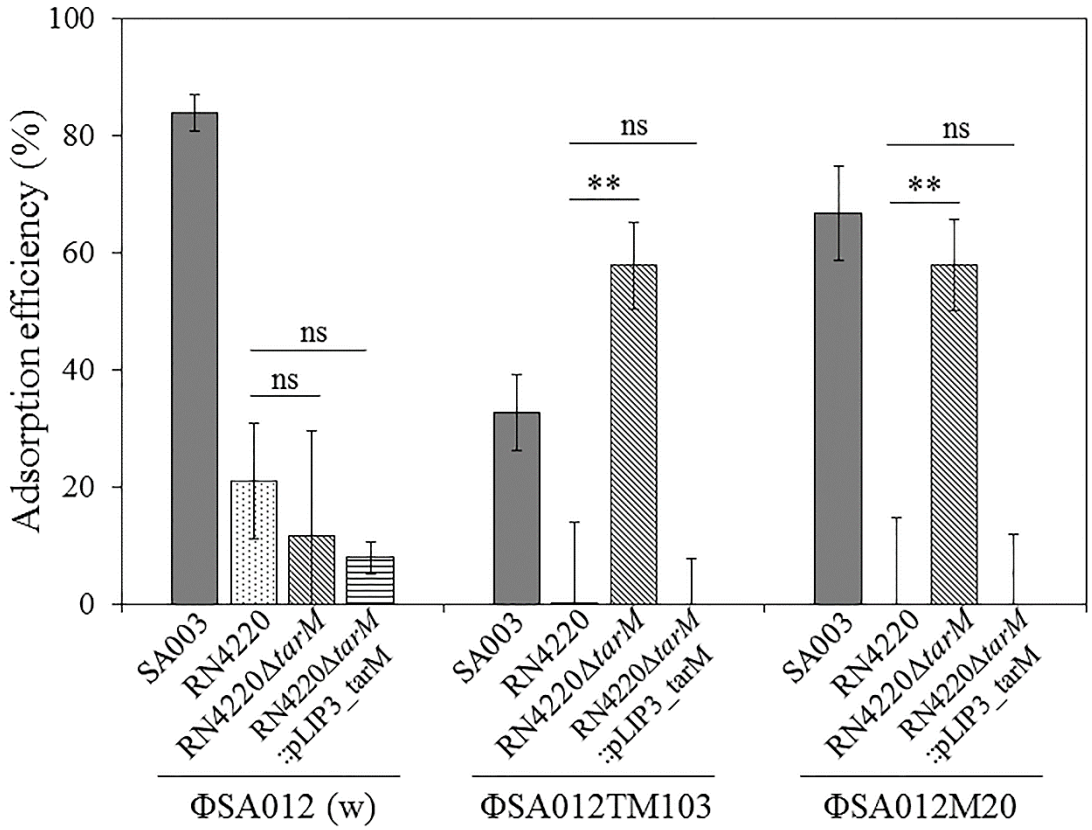


**Figure 6 Adsorption efficiencies of recombinant and mutant phages.**

Adsorption efficiency in $10^8$ CFU/ml of *S. aureus* strains in 60 min. Error bars indicate SD. Three biological replicates were conducted. Asterisks (* and **) indicate statistical significance ($P<0.05$ and $P<0.01$, respectively). ns: not significant.

From these results, it was concluded that ORF103 is the RBP that binds to α-GlcNAc on WTA, and that mutations in ORF103 altered its function, resulting in deficient adsorption of ORF103-mutated phages on *S. aureus* strains whose WTAs contains α-GlcNAc due to the activity TarM. It is plausible that the absence of α-GlcNAc in WTA did not contribute to phage resistance due to the presence of ORF105, previously shown to be an RBP.

### 2.3.5 Effects of anti-ORF103 and anti-ORF105 antibodies on phage infection

To test the hypothesis, it was evaluated the effect of polyclonal antibodies raised against ORF103 and ORF105 on phage infection (Figure 7). Infection of ΦSA012 in RN4220 was drastically inhibited by anti-ORF103 serum, but not in SA003. Inhibition of anti-ORF103 serum was not observed in infection of ΦSA012 in RN4220Δ*tarM*, whereas anti-ORF103 serum inhibited infection of a *tarM*-complemented strain. This indicated that anti-ORF103 serum inhibited the interaction between ORF103 and α-GlcNAc, supporting the idea that ORF103 binds to α-GlcNAc on WTAs and plays an important role in infection only in *S. aureus* strains whose WTAs contain α-GlcNAc.

By contrast, inhibition of anti-ORF105 serum was observed in all *S. aureus* strains (SA003, RN4220, RN4220Δ*tarM*, and RN4220Δ*tarM*::pLIP3_tarM) irrespective of the presence of α-GlcNAc, indicating that ORF105 is the primary RBP in infection of ΦSA012.

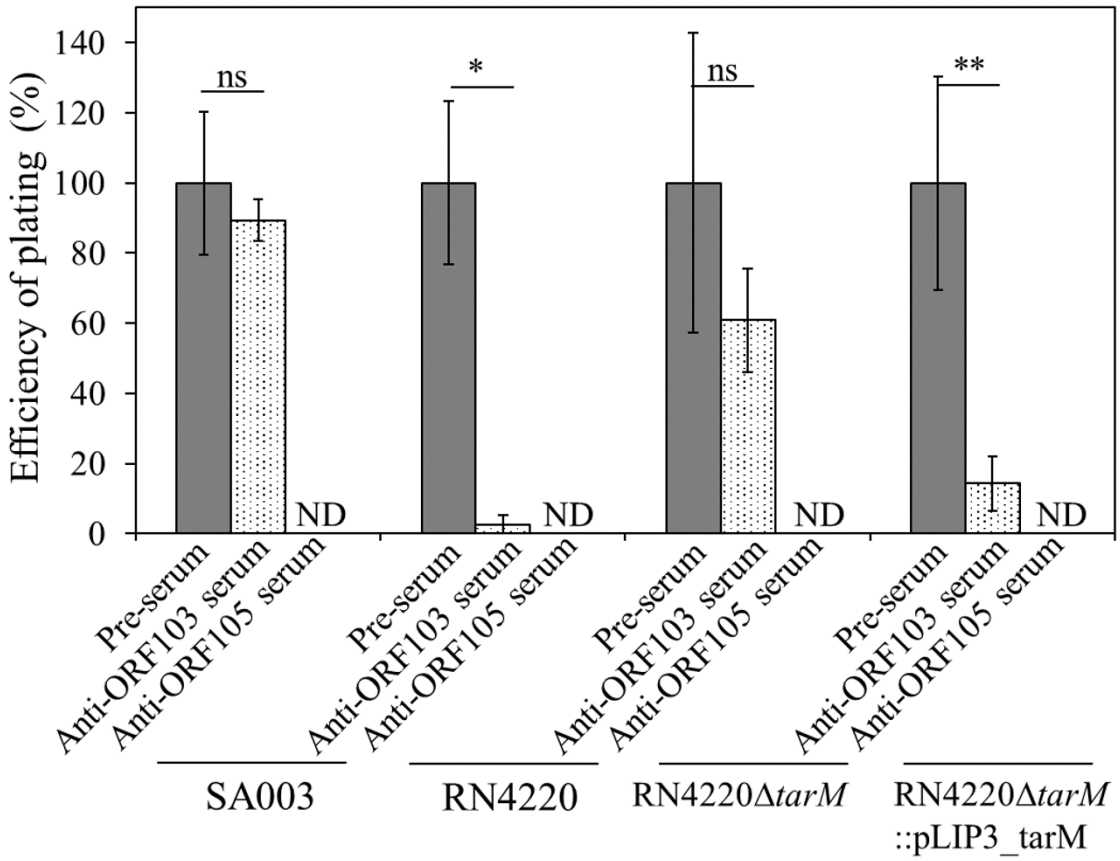


**Figure 7 EOP of ΦSA012 with anti-ORF103 and anti-ORF105 antibodies.**

Pre-immunized serum (Pre-serum) was used in controls. The number of plaques with pre-immunized serum was set as 100%. Plaques were not detected (ND) in the presence of anti-ORF105 serum. Three biological replicates were conducted. Error bars indicate SD. Asterisks (* and **) indicate statistical significance ($P$<0.05 and $P$<0.01, respectively). ns: not significant.

### 2.3.6 Location of ORF103 in ΦSA012

Immunoelectron microscopy using anti-ORF103 antibody and gold-conjugated anti-rabbit antibody revealed that ORF103 in ΦSA012 is localized on the tail fiber at the bottom of the baseplate (Figure 8). This observation supported the hypothesis that ORF103 interacts with components on the cell surface during infection.

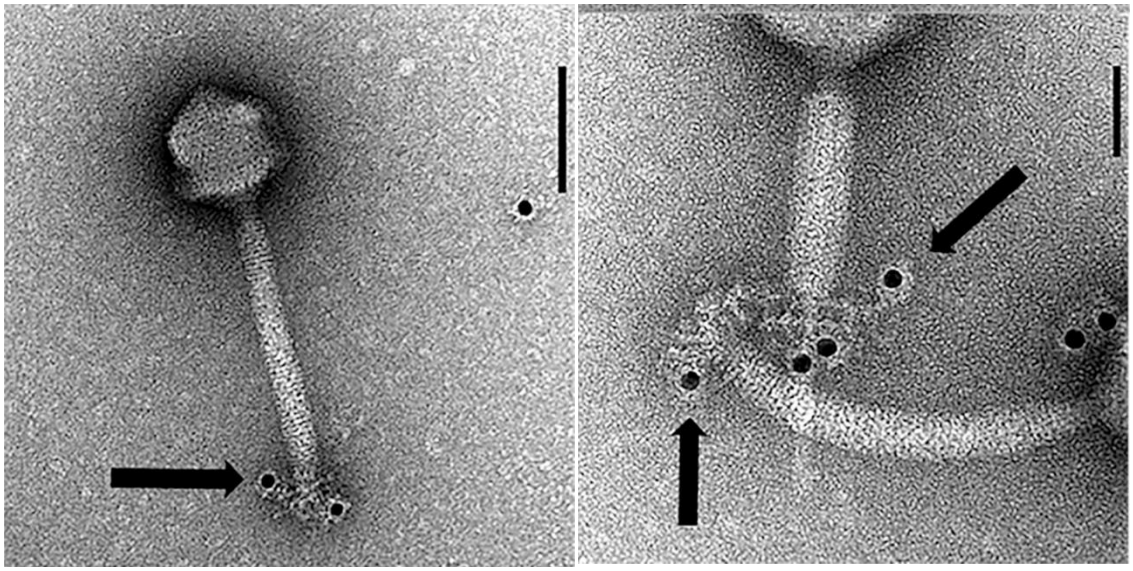

**Figure 8 Localization of ORF103 in ΦSA012 stained with gold-conjugated secondary antibody.**

Black bars indicate 100 nm (left) and 50 nm (right). The size of the gold particles is 12 nm. Black spots in the images represent gold particles conjugated to the secondary antibody. Black arrows indicate the location of the tail fibers in ΦSA012.

### 2.3.7 Effect of three mutations in *orf103* for infection

Apart from the function of ORF103, i.e., binding to α-GlcNAc, mutations in ORF103 seemed to be important during co-evolution between ΦSA012 and SA003. The results of spot test and adsorption assay confirmed that ΦSA012TM103 and ΦSA012M20 could infect the ΦSA012-resistant derivatives SA003R11 and SA003R20, due to the increase in adsorption efficiency caused by the three mutations in *orf103* (Figure 9). The inconsistency in adsorption efficiency between ΦSA012TM103 and ΦSA012M20 suggested that mutations in other genes besides *orf103* also affected adsorption.

The inhibitory effect of anti-ORF103 serum on infection by ΦSA012M20 also suggested that mutated ORF103 is essential for infection of SA003R11 and SA003R20. By contrast, anti-ORF103 serum did not inhibit infection of SA003 (Figure 10). Because WTAs in SA003R11 and SA003R20 do not contain α-GlcNAc due to the absence of *tarM* in these strains, this finding implied that mutations in ORF103 changed the original function of ORF103 to enhance adsorption on ΦSA012-resistant derivatives. Thus, mutations in ORF103 were necessary to adapt to phage resistance arising during co-evolution.

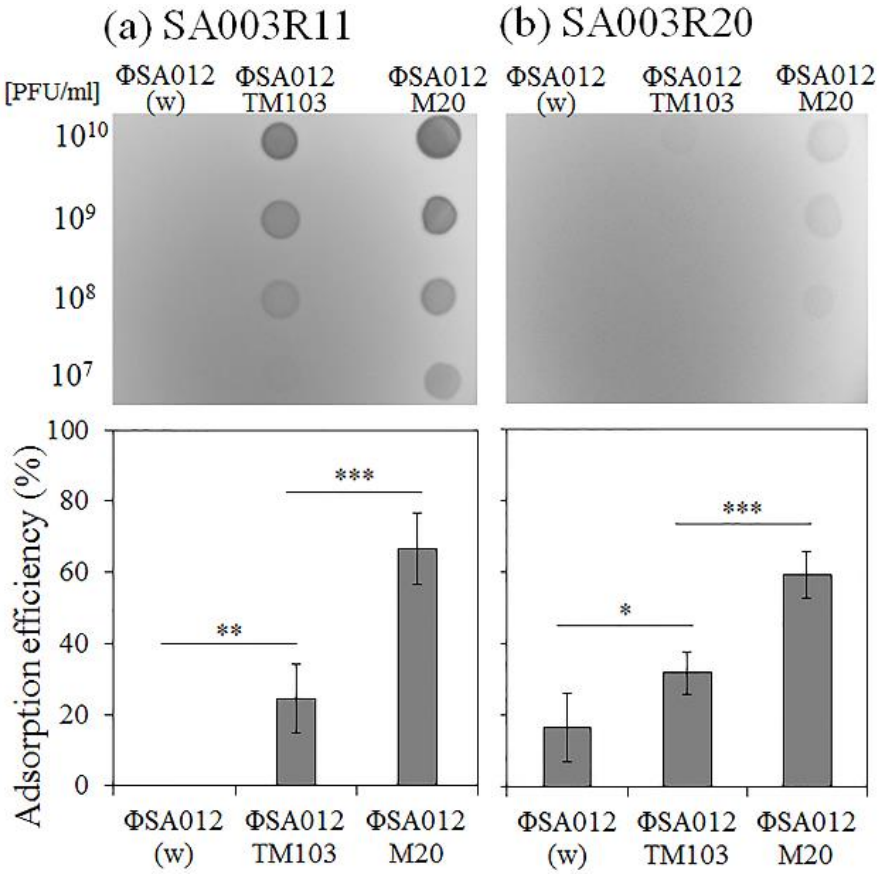


**Figure 9 Spot test and adsorption assay with ΦSA012-resistant strains.**

Upper and lower boxes show the result of adsorption assay ($10^9$ CFU/ml of the cells in 270 min) and spot test, respectively, in (a) SA003R11 and (b) SA003R20. Three or five biological replicates were conducted. Error bars indicate SD. Asterisks (*, **, and ***) indicate statistical significance ($P$<0.05, $P$<0.01, and $P$<0.001, respectively).

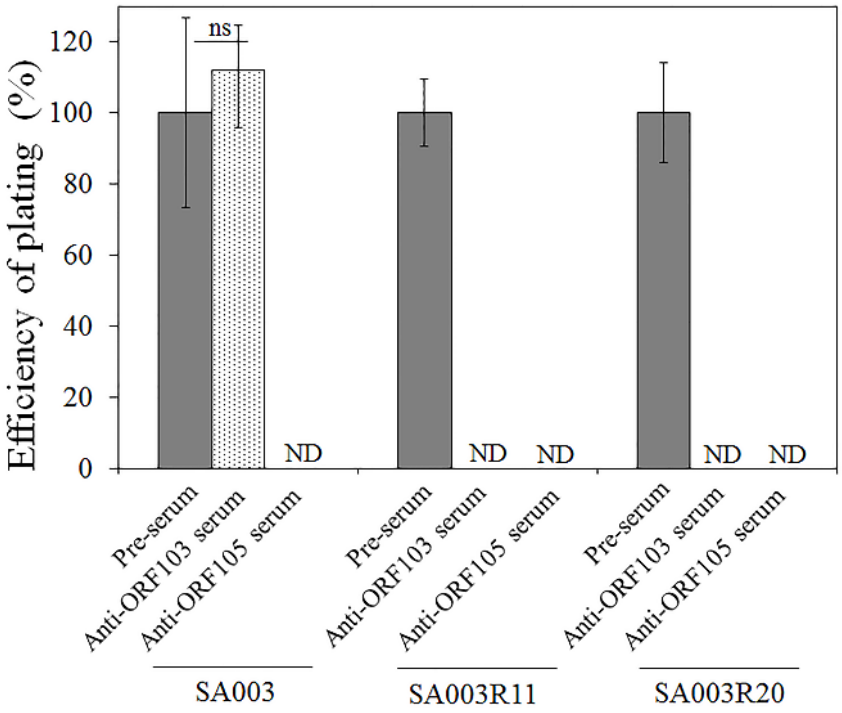


**Figure 10 EOP of ΦSA012M20 with anti-ORF013 and anti-ORF105.**

Pre-immunized serum was used in controls. The number of plaques formed in the presence of pre-immunized serum was defined as 100%. ND: not detected. Three biological replicates were conducted. Error bars indicate SD. ns: not significant.

## 2.4 Discussion

Genomic analysis revealed that ΦSA012 belongs to the genus *Kayvirus* (previously named as *Twortlikevirus*). Until now, more than 80 species of *S. aureus* phages have been reported in the genus *Kayvirus* (e.g., K, ISP, etc.). Phages classified into the genus *Kayvirus* share the following features; (i) large genomes (127-140 kb); (ii) strictly virulent; (iii) a wide host range; and (iv) considerable similarities at the level of protein sequence (43). *Bacillus* phage SPO1, *Listeria* phage A511, *Lactobacillus* phage LP65 (previously named as the genus *SPO1likevirus*), and *Enterococcus* phage ΦEF24C have been considered as related species to phages under the genus *Kayvirus* (54).

Findings in this study showed that at least two adsorption apparatuses (ORF103 and ORF105) are present in ΦSA012. The 37 N-terminal residues of ORF103 and ORF105 are 41% similar. In most cases, the N-termini of RBPs are conserved due to the connection to the virus particle, whereas the C-termini responsible for recognition of the host receptor are diverse. The conserved N-termini of ORF103 and ORF105 may suggest that ORF103 and ORF105 are conjugated with the same virion component. Several phages are known to possess multiple adsorption apparatuses (47). *E. coli* lytic myovirus phi92 has at least five different tail spikes and tail fiber proteins identified by cryoelectron microscopy, allowing it to infect a wide range of *E. coli* and *Salmonella* strains (55). Two different RBPs, LtfA and LtfB of the T5-like siphoviruses DT57C and DT571/2, recognize different O-antigens, the O22 or O87 type and O81 type, respectively (56). Two different carbohydrate-binding modules have been identified in *Lactococcus lactis* phage Tuc2009; the first is in a classical bona fide RBP (BppL), and the other is an accessory protein, BppA (57). BppA enhances adsorption to cells, although its true contribution is not fully understood (58). Considering the aforementioned examples, the presence of multiple RBPs could contributed to the wide host range of *S. aureus* phages in the genus *Kayvirus*.

From the results of spot tests, EOP with antibodies, and adsorption assays, it was

clear that ORF103 is involved in adsorption and binds to α-GlcNAc in WTAs (Figure **5**, Figure 6 and Figure 7). SA003 and RN4220Δ*tarM* were still susceptible to ΦSA012 under inhibition of ORF103 by anti-ORF103 antibody (Figure 7); thus, in the absence of α-GlcNAc, the function of ORF103 is not essential for infection of the host cells by ΦSA012. From the previous studies, *S. aureus* myovirus (including phages under the genus *Kayvirus*) is thought to recognize the backbone of WTA because deletion of *tarM* or *tarS*, which glycosylates α-GlcNAc or β-GlcNAc on WTAs, respectively, did not affect infection of *S. aureus* strains by phage K, whereas the lack of WTAs by deletion of *tagO*, a gene related to the initial step of WTA synthesis, renders *S. aureus* strains resistant to phages (59, 60). In infection by *S. aureus* podovirus, the presence of α-GlcNAc inhibits the adsorption of phages to β-GlcNAc, the podovirus phage receptor, and deletion of TarM enhances phage adsorption (59). Likewise, it is possible that α-GlcNAc masks the backbone of WTAs, which is the binding site for the primary RBP ORF105, and that ORF103 helps the phage bind the WTA backbone by interacting with α-GlcNAc (Figure 11). Hence, phages that lacked wild-type ORF103 function due to point mutations or antibodies were not able to infect *S. aureus* strains in the presence of α-GlcNAc, whereas loss of ORF103 function did not affect phage infection in the absence of α-GlcNAc. The reason why ΦSA012 did not adsorb stronger to RN4220 which possesses α-GlcNAc in WTA than RN4220ΔtarM lacking α-GlcNAc in WTA might be that the presence of α-GlcNAc inhibits the binding of ORF105 to the backbone of WTA even though the binding of ORF103 to α-GlcNAc could contribute to adsorption efficiency of ΦSA012 (Figure 6). The influence of β-GlcNAc in adsorption may be minor, as no inhibition of infection by the anti-ORF103 antibody was observed in SA003 irrespective of the presence of *tarS*, which is responsible for glycosylation of β-GlcNAc.

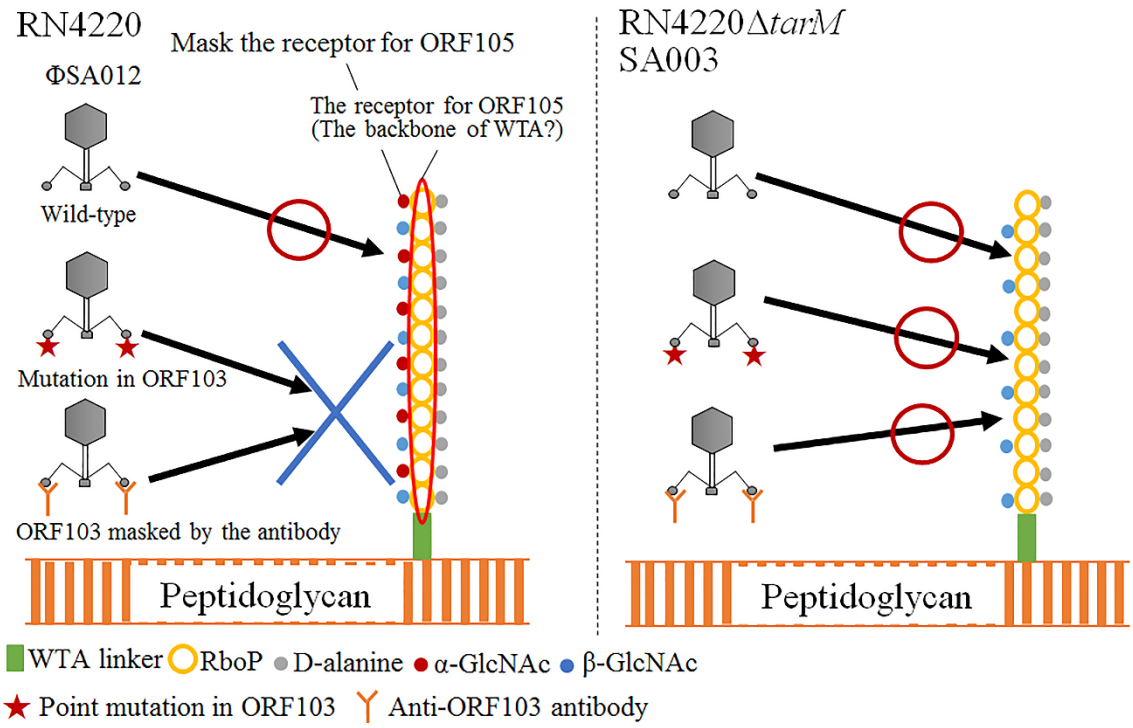


**Figure 11 Scheme of putative adsorption mechanism of ΦSA012.**

In most *S. aureus* strains, the WTA polymer consists of 11-40 ribitol phosphate (RboP) repeats substituted with D-alanine and α- and β-GlcNAc, covalently attached to a peptidoglycan with a WTA linkage unit. ΦSA012 recognizes the WTA backbone. α-GlcNAc masks the WTA backbone, which is the binding site of the primary RBP ORF105, and ORF103 helps the phage bind the WTA backbone by binding α-GlcNAc. Hence, a phage in which ORF103 is disabled by point mutations or antibodies cannot infect *S. aureus* strains in the presence of α-GlcNAc, whereas loss of ORF103 function does not affect phage infection in the absence of α-GlcNAc.

# CHAPTER 3 ANALYSES OF PROPAGATION PROCESSES OF *S. aureus* PHAGES

## 3.1 Introduction

In Chapter 2, *S. aureus* phage ΦSA012 was characterized to understand general features of phages as one of promising candidates for phage therapy. It was revealed that the wide host range of *S. aureus* phages in the genus *Kayvirus* is attributed to the presence of multiple RBPs. In addition to ΦSA012, a wide variety of phages have been reported for the potentially therapeutic purpose (61). For example, *S. aureus* lytic phages S13′ and S25-3 can be considered as promising candidates for phage therapy because these two phages had a broad host range and strong lytic activity on a broad range of *S. aureus* strains (14). While phage S25-3 is classified into the genus *Kayvirus* as well as ΦSA012, phage S13′ is classified into the genus *Rosenblumvirus*. In addition to phages S13′ and S25-3, *S. aureus* phages in two genera *Rosenblumvirus* and *Kayvirus* are considered to be potential therapeutic candidates due to their strong lytic effects and broad host ranges (61). Due to their different mechanisms of host recognition in genera *Rosenblumvirus* and *Kayvirus*, the infectivity against *S. aureus* is different in these two groups of phages (39, 62). Since the infectivity of phages is specific compared to the antibiotics, it is important to combine various types of *S. aureus* phages and widen the spectrum against *S. aureus* strains (63). Thus, several types of *S. aureus* phages need to be manufactured for the treatment of *S. aureus* infections.

For phage production, the theoretical models have been developed and widely discussed under the universal concept of host-virus interactions (64-66). However, knowledge of the propagation for *S. aureus* phages is missing in the three points below. First, the difference in propagation by characters of *S. aureus* phages has not been investigated experimentally, while several types of *S. aureus* phages are needed to be manufactured for the reasons mentioned above. Second, key process parameters in the manufacturing should be clarified. Although the mathematical models of phage

propagation have been constructed based on the kinetic parameters (adsorption constant, burst size, latent period, etc.), these kinetic parameters are influenced by culture conditions (temperature, bacterial status, substrate concentration, etc.) and difficult to be directly manipulated themselves (67-69). It is necessary for control of manufacturing to clarify the key process parameters to be regulated (22). Third, adequate methodologies to quantify the phage concentration after the propagation process have not been discussed, although the plaque assay and quantitative PCR (qPCR) are typically used for virus concentration measurements (70).

This chapter describes the evaluation for the difference of propagation by characteristics of *S. aureus* phages and their key process parameters on propagation with two different types of *S. aureus* phages S13′ and S25-3. In order to measure the effects of process parameters, phage culture experiments of phages S13′ and S25-3 were conducted in a flask by using, a new class of design of experiment (DoE), definitive screening design (DSD), which is a statistical and mathematical tool to clarify the relationship between process parameters and responses with a minimized number of experiments (71). The phage concentrations were measured by the plaque assay and qPCR, and the results were compared.

## 3.2 Materials and Methods

### 3.2.1 Bacteria, phages, culture conditions, and reagents

*S. aureus* strain SA27 was used for propagation and enumeration of *S. aureus* phages as a host bacterial strain (12). *S. aureus* phages S13′ and S25-3 have been reported previously (14). *E. coli* strain DH5α (Takara Bio, Shiga, Japan) was used for cloning.

LB broth (LB Medium (Miller); Kanto Chemical Co., Inc., Tokyo, Japan) was used to culture bacteria and phages. If required, ampicillin at 100 μg/ml was added to the culture medium. Bacteria and phages were cultured at 37°C unless otherwise stated. All

reagents were purchased from Nacalai Tesque (Kyoto, Japan) or Fujifilm Wako Pure Chemical Corporation (Osaka, Japan) unless otherwise stated.

Bacterial density was measured in CFU/ml. Phage concentration was measured using the double-layered agar method in PFU/ml unless otherwise stated (72).

### 3.2.2 The measurement of adsorption efficiencies and burst sizes

For the measurement of adsorption efficiencies, bacteria at $3.0 \times 10^8$ CFU/ml were mixed with phages at $3.0 \times 10^4$ CFU/ml in 20 ml of LB broth, and the mixture was cultured with shaking. At 1, 5, 10, and 15 min after mixing phages and bacteria, 500 μl of bacteria-phage culture was mixed with an equal volume of chloroform. After centrifugation (15,000 ×*g*, 30 s, room temperature), the supernatant was collected and the plaque assay was performed.

In order to measure burst sizes and latent periods, bacteria at $3.0 \times 10^7$ CFU/ml and $3.0 \times 10^6$ CFU/ml were mixed with phages S13′ and S25-3 at $3.0 \times 10^2$ PFU/ml, respectively, in 20 ml of LB broth. After 5 min incubation at 37°C with shaking, the culture suspension was centrifuged (15,000 ×*g*, 1 min, room temperature) and the supernatant was replaced with 10 ml of prewarmed LB broth at 37°C. The bacteria-phage culture was continuously cultured with shaking. The culture was sampled over time, and the plaque assay was performed.

### 3.2.3 Extraction of phage genomic DNA

The phage suspension supplemented with 10 mM $MgCl_2$ was incubated with 20 μg/ml of DNase I and RNase A at 37°C for 30 min and was then incubated at 75°C for 5 min. Phage suspension was then incubated in protein-digestive solution (5 μg/ml of proteinase K (Takara Bio), 0.5% sodium dodecyl sulfate, 100 mM EDTA, 100 mM Tris-HCl, pH 7.8) at 56°C for 1 h. DNA extraction was done by phenol-chloroform extraction and ethanol precipitation, as described elsewhere (73, 74).

### 3.2.4 qPCR

Primers and probes were designed for each genomic region encoding a capsid protein. The genome sequences of phages S13′ and S25-3 were obtained from GenBank (accession numbers, AB626963 and AB853330, respectively) (39, 75). All primers and probes labeled with FAM and TAMRA are described in Table 5.

**Table 5 The list of primers for qPCR.**

| Primers/Probes | | Direction | Sequence (5' → 3')[a] | Description |
|---|---|---|---|---|
| pUC_linear | pUC_linear_F2 | Forward primer | GATCCTCTAGAGTCGACCTGCAGG | The primers were used to amplify the pUC19 plasmid sequence to obtain a linearized plasmid for cloning. The amplified DNAs were used to clone DNA sequences of phages S13′ and S25-3. |
| | pUC_linear_R2 | Reverse primer | GATCCCCGGGTACCGAGCTC | |
| S13′_Inf | S13′_Inf_F | Forward primer | CGGTACCCGGGGATCCAATTTCCAAACATTAGCAGAC | The primers were used to amplify the phage S13′ sequence for the construction of a plasmid carrying the phage S13′ sequence. The plasmid was used as a standard to quantify the copy number of phage S13′. |
| | S13′_Inf_R | Reverse primer | CGACTCTAGAGGATCGGAAAGTGTTCGCAATCTTTGTATC | |
| S25-3_Inf | S25-3_Inf_F | Forward primer | CGGTACCCGGGGATCTGGTTATGGAATCACTCCTG | The primers were used to amplify the phage S25-3 sequence for the construction of a plasmid carrying the phage S25-3 sequence. The plasmid was used as a standard to quantify the copy number of phage S25-3. |
| | S25-3_Inf_R | Reverse primer | CGACTCTAGAGGATCGGAATGAAGCCCACTCAATTG | |
| qPCR-S13′ | F_S13′ | Forward primer | AATGCGTGCGATGTTAGTTG | The set of primers and probes was used to quantify the copy number of phage S13′. |
| | R_S13′ | Reverse primer | ATATTGCCCAATTGCACCAC | |
| | S13′_qPCR_P | Probe | (FAM)-CATCAAAACAAGATTTAGCAAGTAAAG-(TAMRA) | |
| qPCR-S25-3 | F_S25-3 | Forward primer | GTATCTGACCCAAATATCCGTC | The set of primers and probes was used to quantify the copy number of phage S25-3. |
| | R_S25-3 | Reverse primer | GAATGAAGCCCACTCAATTG | |
| | S25-3_P | Probe | (FAM)-GACCCATCACAAATCCTTACAG-(TAMRA) | |

[a] Underlines indicate the overlap sequence for the fusion of fragments by In-Fusion cloning technology (Takara Bio).

Plasmids containing reference sequences were constructed to calculate the copy numbers of DNA. Using appropriate primer sets, the DNA fragments of phages and pUC19 plasmid were amplified using PCR with phage genomic DNAs and pUC19 plasmid (Takara Bio), respectively. These amplified fragments were fused using an In-Fusion HD cloning kit (Takara Bio). The exact phage sequences were cloned into pUC19 in *E. coli* strain DH5α. Plasmid extraction was conducted using a plasmid DNA extraction kit (Favorgen Biotech Co., Ping-Tung, Taiwan).

For each qPCR reaction, 20 μl of the reaction mixture was prepared with 10 μl of 2 × Premix Ex Taq (Takara Bio), 0.4 μl of each 10 mM primer, 0.8 μl of a TaqMan probe, 0.2 μl of 50 × ROX Reference Dye II (Takara Bio), 1 μl of DNA template (≈$10^6$-fold diluted in water as needed) and 7.6 μl of water. Subsequently, PCR was performed using a 7500 Real-time PCR System (Applied Biosystems, Foster City, CA, USA), using the following program: initial denaturation at 95°C for 30 s, and 35 cycles of two-step amplification (95°C for 5 s, 50°C for 30 s). Reactions without template DNA were performed as a negative control. The results of qPCR were analyzed with 7500 Software version 2.0.6 (Applied Biosystems).

### 3.2.5 Design of experiments and data analysis

DoE and all statistical analyses were performed using JMP statistical software (version 15.0) (SAS Institute, Cary, NC, USA).

The experimental conditions of phage culture experiments were designed using DSD, and the regression models of the results were generated using the equation,

$$y = \beta_0 + \sum_i^k \beta_i x_i + \sum_{i>j}^k \beta_{ij} x_i x_j + \sum_i^k \beta_{ii} x_i^2,$$

where $y$ is the response, $x$ represents the parameters, $k$ is the number of parameters, $\beta_0$ is the intercept, and $\beta_i$, $\beta_{ij}$, and $\beta_{ii}$ are the regression coefficients for the main effects, the

two-factor interactions, and the quadratic effects, respectively. The selection of active effects was conducted as previously described (76). All effects with a *P* value of more than 0.05 were removed from the models.

### 3.2.6 Selection of process parameters

For selection of process parameters to be studied, baculovirus production was referred as the model for the propagation process of phage production because host cells for both of baculovirus and phages are suspension cells. According to knowledge from baculovirus production, key process parameters for propagation include MOI, bacterial density at infection (BDI), time of harvest (TOH), and temperature (77, 78).

### 3.2.7 Phage culture experiments using 200-ml Erlenmeyer flasks

Following the experimental design process using DSD, the phage culture experiments were performed. Three levels at regular intervals (i.e., low, middle, and high) were set for each process parameter. To prepare the suspension of host bacterial culture for the phage culture experiment, 3 ml of an overnight culture of *S. aureus* strain SA27 was inoculated into 300 ml of LB broth in a 1,000-ml Erlenmeyer flask, and was cultured with stirring at 37°C for 16 h at 500 rpm by a 3.5-cm stirring bar (AS ONE, Osaka, Japan) using an electromagnetic stirrer (AS ONE). Bacterial culture at three levels of defined bacterial density (i.e., $10^6$, $10^7$, or $10^8$ CFU/ml) was prepared by diluting the overnight culture with culture media by using the equation shown in Figure 12.

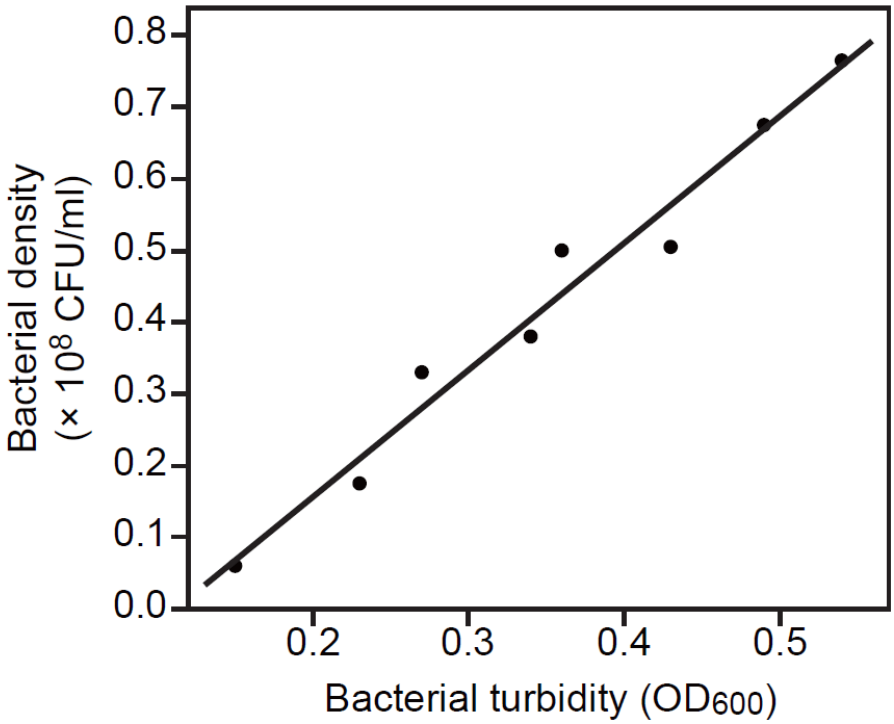


**Figure 12 The correlation of bacterial density with bacterial turbidity in *S. aureus* culture in the midexponential phase.**

The bacterial density was measured in CFU/ml. The bacterial turbidity was measured at $OD_{600}$. Analyzing the dataset by linear regression, the line was fitted, giving $y = -0.3591 + 7.62x$ and the coefficient of determination (i.e., $R^2$) was 0.759.

After the addition of a phage suspension at the defined concentrations (i.e., MOI: $10^{-3}$, $10^{-2}$ or $10^{-1}$), 50 ml of bacteria-phage culture was incubated at each defined temperature (i.e., 34, 37, or 40°C) in a 200-ml Erlenmeyer flask with a water-bath shaker (Taitec Co., Saitama, Japan) at 150 rpm shaking speed.

After incubating for a defined duration (i.e., 2, 4, or 6 h), the bacteria-phage culture was centrifuged (5,000 ×*g*, 5 min, 4°C) and then the supernatant was filtered with a 0.45-μm syringe filter (Sartorius, Goettingen, Germany). Finally, the concentration of phage suspension was measured using the plaque assay and qPCR, as described above.

## 3.3 Results

### 3.3.1 Adsorption efficiencies, burst sizes, and latent periods

Before the evaluation of the propagation processes of two phages, adsorption efficiency, burst size, and latent period were compared in phages S13′ and S25-3 in order to assess the propagation performance of phages (Figure 13). For phage S13′, the phages adsorbed within 15 min, the latent period, and the burst size were 99.56% ± 0.08%, 40 min, and 99 ± 18 (mean ± standard deviation (SD)), respectively. For phage S25-3, the phages adsorbed within 15 min, the latent period, and the burst size were 98.60% ± 0.62%, 40 min, and 43 ± 8.1, respectively. According to these results, phage S13′ exhibited a higher adsorption efficiency and a larger burst size in *S. aureus* strain SA27 than phage S25-3, while latent periods were equivalent to both phages. These data suggest that phage S13′ possesses higher efficiency of propagation than phage S25-3 in *S. aureus* strain SA27.

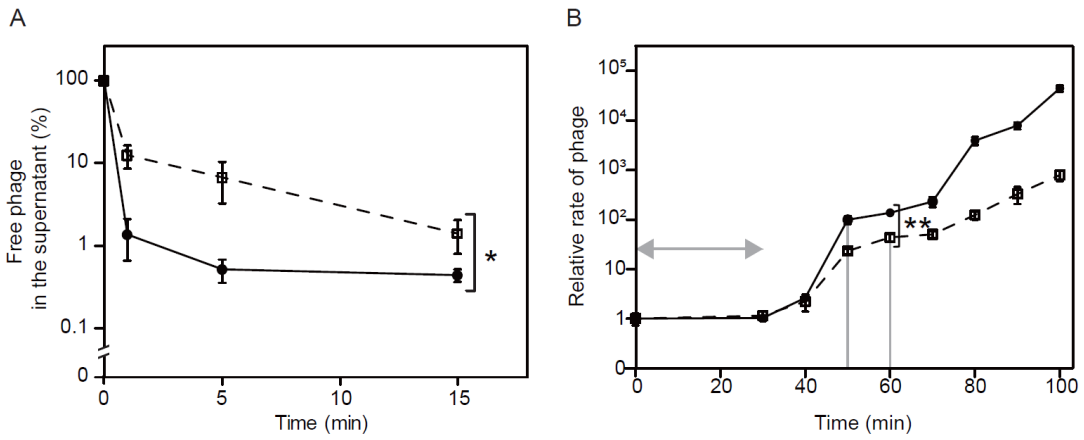


**Figure 13 Adsorption efficiencies, burst sizes, and latent periods of phages S13′ and S25-3 on *S. aureus* strain SA27.**

(A) Adsorption rate. (B) Burst sizes and latent periods. Closed circle (●) with a straight line and open square (□) with a dotted line represent the mean value of phages S13′ and S25-3, respectively. Error bars on each dot represent SD. In (B), the vertical gray lines indicate the points for burst sizes. The horizontal gray line with arrow heads on both ends indicates the latent period. The experiment was performed in triplicate. Asterisks indicate statistical significance (**and *, $P < 0.001$ and 0.05, respectively).

### 3.3.2 Methodologies for the plaque assay and qPCR

In order to quantify the number of phages, the plaque assay and qPCR are applied in this study. While the plaque assay is a popular method in phage research, qPCR is also popular method for detection and quantification of viruses due to its technical simplicity and shorter processing time (70, 79). The plaque assay measures active phages as titer in PFU/ml, while qPCR measures viral genome copy (VGC) in copy/ml, where the copies are derived from both active and nonactive phage particles. To observe technical differences between the plaque assay and qPCR, the correlation between titers and VGCs was examined in phages S13′ and S25-3 (Figure 14). The relationship between titers and VGCs was confirmed, and the values of titers and VGCs were very similar for both phages.

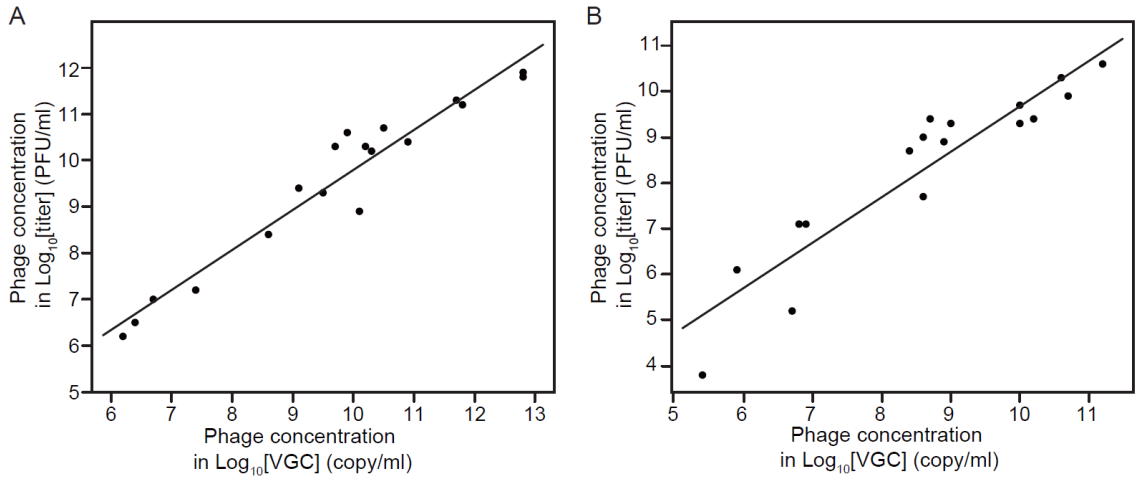


**Figure 14 The correlation of bacterial density with bacterial turbidity in *S. aureus* overnight culture.**

Correlation of phage concentrations in $Log_{10}$[titer] with that in $Log_{10}$[VGC]. (A) Phage S13′. Analyzing the dataset of phage S13′ by linear regression, the line was fitted, giving $y = 0.8644x + 1.148$ and the coefficient of determination (i.e., $R^2$) was 0.938. (B) Phage S25-3. Analyzing the dataset of phage S25-3 by linear regression, the line was fitted, giving $y = 0.9919x - 0.2456$ and $R^2$ was 0.879.

### 3.3.3 The design of phage culture experiments by using DSD

From the established models of host-virus interactions, four key process parameters for propagation were selected and examined in this study: MOI, BDI, TOH, and temperature (80-83). Because the magnitudes of MOI and BDI were shown as a power of 10, they were transformed by base 10 logarithm (i.e., $Log_{10}$[MOI] and $Log_{10}$[BDI]). In addition, because the phage generally multiplies exponentially, the phage concentrations of titer and VGC were also transformed by base 10 logarithm, i.e., $Log_{10}$[titer] and $Log_{10}$[VGC], in this study.

Using DSD, 17 runs with different values of process parameters were designed (Table 6). In DSD, when the number of parameters is less than five ($k < 5$), the minimum number of experiments is 13 runs, while $2k + 1$ and $2k + 3$ runs are the minimum numbers of experiments when $k$ is even and odd numbers, respectively. In addition, as recommended by Jones and Nachtsheim, four extra runs were randomly added to increase the ability to detect second-order effects (84).

**Table 6 Experimental design by DSD and experimental results.**

| Experimental design determined by DSD | | | | | Experimental result | | | |
|---|---|---|---|---|---|---|---|---|
| Run No.[a] | $Log_{10}$[MOI] | $Log_{10}$[BDI] (CFU/ml) | TOH (h) | Temperature (°C) | Phage S13′ concentration | | Phage S25-3 concentration | |
| | | | | | $Log_{10}$[titer] (PFU/ml) | $Log_{10}$[VGC] (copy/ml) | $Log_{10}$[titer] (PFU/ml) | $Log_{10}$[VGC] (copy/ml) |
| 1 | -3 | 6 | 2 | 40 | 6.2 | 6.2 | 3.8 | 5.4 |
| 2 | -1 | 7 | 6 | 40 | 10.2 | 10.3 | 9.3 | 10.0 |
| 3 | -1 | 8 | 6 | 34 | 11.3 | 11.7 | 9.7 | 10.0 |
| 4 | -2 | 8 | 6 | 40 | 11.8 | 12.8 | 10.6 | 11.2 |
| 5 | -1 | 8 | 2 | 34 | 10.4 | 10.9 | 9.4 | 10.2 |
| 6 | -1 | 6 | 6 | 34 | 9.3 | 9.5 | 8.9 | 8.9 |
| 7 | -2 | 7 | 4 | 37 | 10.6 | 9.9 | 9.4 | 8.7 |
| 8 | -3 | 6 | 6 | 40 | 10.3 | 10.2 | 9.9 | 10.7 |
| 9 | -3 | 8 | 4 | 34 | 11.2 | 11.8 | 10.3 | 10.6 |
| 10 | -1 | 8 | 2 | 40 | 8.9 | 10.1 | 7.7 | 8.6 |
| 11 | -2 | 6 | 2 | 34 | 6.5 | 6.4 | 6.1 | 5.9 |
| 12 | -3 | 6 | 6 | 34 | 10.3 | 9.7 | 9.0 | 8.6 |
| 13 | -3 | 8 | 6 | 37 | 11.9 | 12.8 | 10.6 | 11.2 |
| 14 | -3 | 8 | 2 | 40 | 7.2 | 7.4 | 5.2 | 6.7 |
| 15 | -1 | 6 | 4 | 40 | 9.4 | 9.1 | 8.7 | 8.4 |
| 16 | -3 | 7 | 2 | 34 | 7.0 | 6.7 | 7.1 | 6.8 |
| 17 | -1 | 6 | 2 | 37 | 8.4 | 8.6 | 7.1 | 6.9 |

[a] Run No. 7 is the center point in this experimental design.

As per the experimental design using DSD, phage culture experiments were performed and phage concentrations were measured using the two methodologies of the plaque assay and qPCR. Analyzing the distribution of obtained data in this study, the scatter plot of phage concentration in $Log_{10}$[titer] or $Log_{10}$[VGC] over each key process parameter (i.e., MOI, BDI, TOH or temperature) showed that no data were present outside the 95% confidence area, which suggested that outliers were not present in these datasets (Figure 15). Thus, regression models of phage propagation could be generated from the datasets.

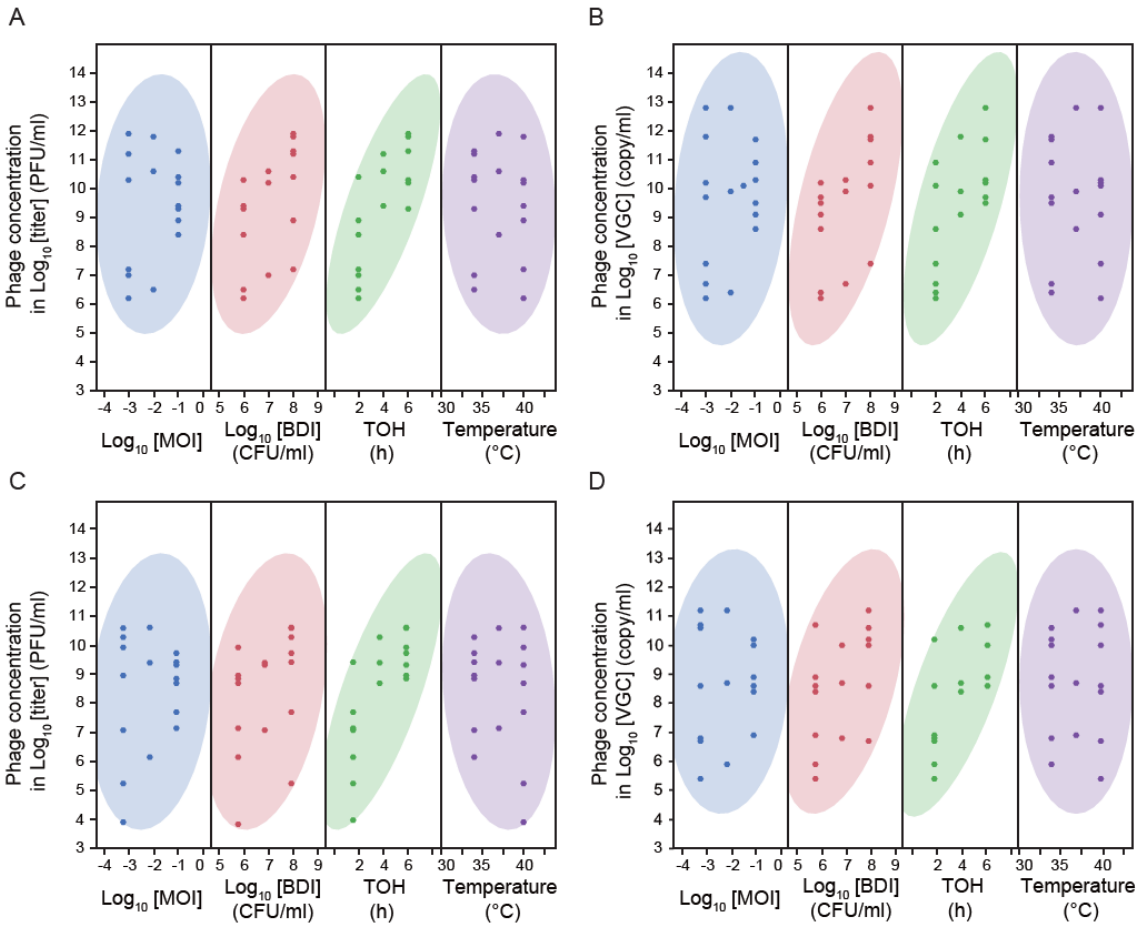


**Figure 15 Scatter plot of phage concentration against key process parameters.**

Scatter plots of phage concentrations in phages S13′ and S25-3 against key process parameters are shown. (A) $Log_{10}$[titer] and (B) $Log_{10}$[VGC] of phage S13′ were indicated, whereas (C) $Log_{10}$[titer] and (D) $Log_{10}$[VGC] of phage S25-3. The key process parameters are $Log_{10}$[MOI], $Log_{10}$[BDI], TOH, and temperature. Shaded areas indicate 95% confidence, which was calculated from the bivariate normal distribution. Because no data were present outside the 95% confidence area, outliers were not considered to be present in these datasets.

### 3.3.4 Regression model for phage S13′ propagation

In the analysis of the regression model of phage S13′ propagation, the process parameters critical for phage propagation were then statistically screened. In the regression models of phage concentrations in $Log_{10}$[titer] and $Log_{10}$[VGC], the $Log_{10}$[BDI] and TOH were included with statistical significance (Figure 16 and Figure 17). In these regression models, both phage concentrations in $Log_{10}$[titer] and $Log_{10}$[VGC] were positively related to $Log_{10}$[BDI] and TOH. Two-parameter interactions and quadratic effects were not observed in the regression models.

The formulas of the regression model of phage S13′ concentrations in $Log_{10}$[titer] and $Log_{10}$[VGC] are as follows:

$$\mathrm{Log}_{10}[\mathrm{titer}] = 9.46 + 0.88 \times (\mathrm{Log}_{10}[\mathrm{BDI}] - 7) + 0.73 \times (\mathrm{TOH} - 4), \text{ and}$$

$$\mathrm{Log}_{10}[\mathrm{VGC}] = 9.65 + 1.27 \times (\mathrm{Log}_{10}[\mathrm{BDI}] - 7) + 0.74 \times (\mathrm{TOH} - 4).$$

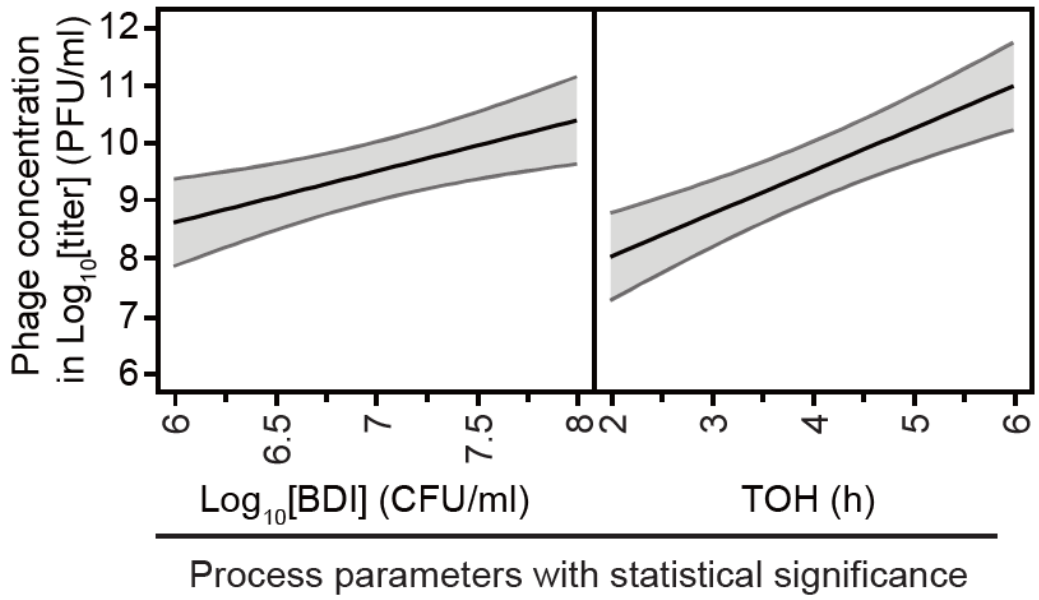


| Effect | Estimate | Standard error | *t* ratio | *P* value |
|---|---|---|---|---|
| $Log_{10}$[BDI] | 0.88 | 0.26 | 3.39 | 0.0044 |
| TOH | 1.46 | 0.26 | 5.65 | <0.0001 |

**Figure 16 Interaction profiles of the regression model of phage S13′ propagation ($Log_{10}$[titer]).**

In the top panels, the interaction plots of phage concentration with process parameters detected in the regression models are shown. In the interaction plots, the line segments with gray areas are shown as possible interactions with 95% confidence. On the bottom, the process parameters that interacted with phage concentrations with statistical significance are shown as a table. In the table, the results provided by regression analysis, including *P* values, are shown.

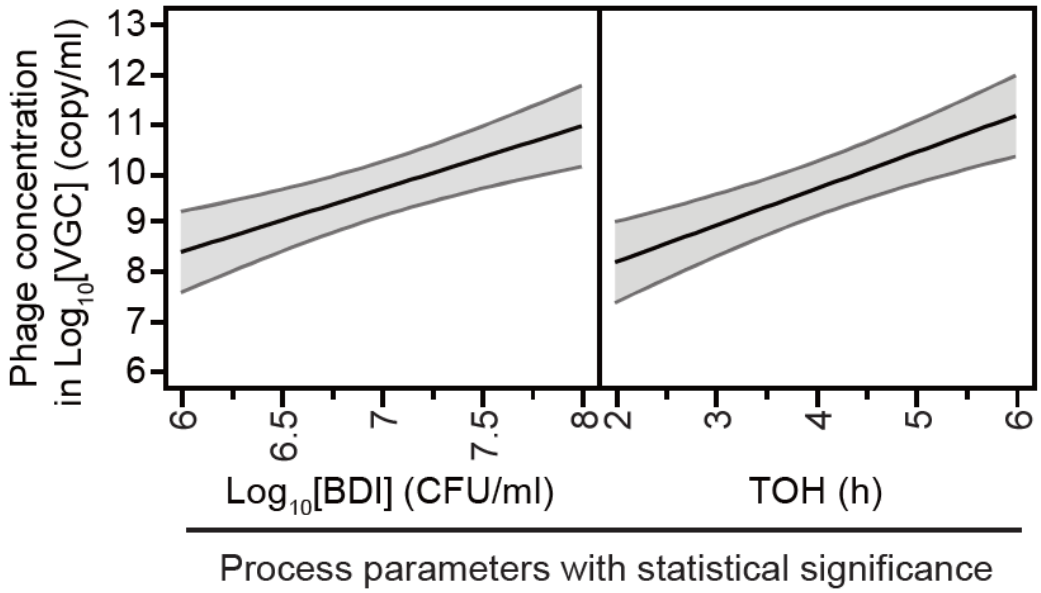


| Effect | Estimate | Standard error | *t* ratio | *P* value |
|---|---|---|---|---|
| $Log_{10}$[BDI] | 1.27 | 0.28 | 4.50 | 0.0005 |
| TOH | 1.48 | 0.28 | 5.23 | 0.0001 |

**Figure 17 Interaction profiles of the regression model of phage S13′ propagation ($Log_{10}$[VGC]).**

In the top panels, the interaction plots of phage concentration with process parameters detected in the regression models are shown. In the interaction plots, the line segments with gray areas are shown as possible interactions with 95% confidence. On the bottom, the process parameters that interacted with phage concentrations with statistical significance are shown as a table. In the table, the results provided by regression analysis, including *P* values, are shown.

### 3.3.5 Regression model for phage S25-3 propagation

The regression model for phage S25-3 propagation was analyzed in the same manner as the analysis of phage S13′ propagation. Unlike the regression models of phage S13′ propagation in $Log_{10}$[titer], finding the regression model of phage S25-3 propagation was not simple (Figure 18). The model included main effects by $Log_{10}$[MOI], $Log_{10}$[BDI], TOH, and temperature, two-factor interactions by $Log_{10}$[MOI] × TOH and TOH × temperature, and a quadratic effect by TOH × TOH, with statistical significance. First, positive relationships of phage concentrations in $Log_{10}$[titer] with $Log_{10}$[MOI] and $Log_{10}$[BDI] were observed. Second, a positive relationship of phage concentration in $Log_{10}$[titer] was observed with TOH from 2 to 4 h but leveled off from 4 to 6 h. Third, a negative relationship was observed with temperature. Fourth, two-factor interactions of $Log_{10}$[MOI] × TOH and TOH × temperature were also included.

In contrast, as seen in the regression model of phage S13′ propagation in $Log_{10}$[VGC], the regression model of phage S25-3 propagation in $Log_{10}$[VGC] was simple (Figure 19), only including $Log_{10}$[BDI] and TOH with statistical significance. Positive relationships of phage concentration in $Log_{10}$[VGC] with $Log_{10}$[BDI] and TOH were observed. Two-factor interactions and quadratic effects were not observed in the analysis.

The formulas of regression models of phage S25-3 concentrations in $Log_{10}$[titer] and $Log_{10}$[VGC] in phage propagation were obtained as follows:

$$\begin{aligned}\mathrm{Log_{10}[titer]} &= 6.62 + 0.35 \times \mathrm{Log_{10}[MOI]} + 0.71 \times \mathrm{Log_{10}[BDI]} + \\ &0.77 \times \mathrm{TOH} + 0.12 \times \mathrm{Temperature} + (\mathrm{Log_{10}[MOI]} + 2) \times (\mathrm{TOH} - \\ &4) \times (-0.36) + (\mathrm{TOH} - 4) \times (\mathrm{Temperature} - 37) \times 0.09 + (\mathrm{TOH} - \\ &4) \times (\mathrm{TOH} - 4) \times (-0.32), \text{ and}\end{aligned}$$

$$\mathrm{Log_{10}[VGC]} = (-0.97) + 0.98 \times \mathrm{Log_{10}[BDI]} + 0.72 \times \mathrm{TOH}.$$

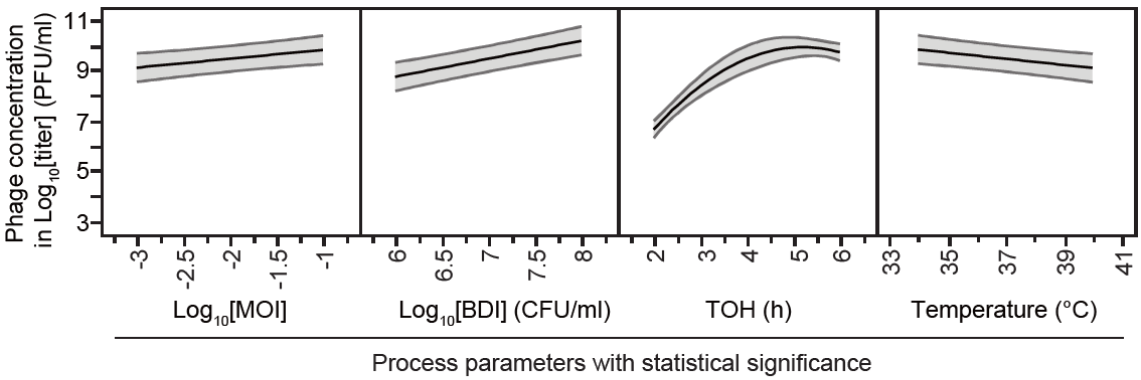


| Effect | Estimate | Standard error | *t* ratio | *P* value |
|---|---|---|---|---|
| $Log_{10}$[MOI] | 0.35 | 0.11 | 3.36 | 0.0084 |
| $Log_{10}$[BDI] | 0.71 | 0.11 | 6.79 | <0.0001 |
| TOH | 0.77 | 0.05 | 14.56 | <0.0001 |
| Temperature | -0.12 | 0.04 | -3.49 | 0.0069 |
| $Log_{10}$[MOI] × TOH | -0.36 | 0.06 | -6.19 | 0.0002 |
| TOH × Temperature | 0.09 | 0.02 | 4.89 | 0.0009 |
| TOH × TOH | -0.32 | 0.06 | -5.09 | 0.0007 |

**Figure 18 Interaction profiles of the regression model of phage S25-3 propagation ($Log_{10}$[titer]).**

In the regression models of phage S25-3 propagation, phage concentrations were analyzed in $Log_{10}$[titer]. In the top panels, the interaction plots of phage concentration with process parameters detected in the regression models are shown. In the interaction plots, the line segments with gray areas are shown as possible interactions with 95% confidence. On the bottom, the process parameters that interacted with phage concentrations with statistical significance are shown as a table. In the table, the results provided by regression analysis, including *P* values, are shown.

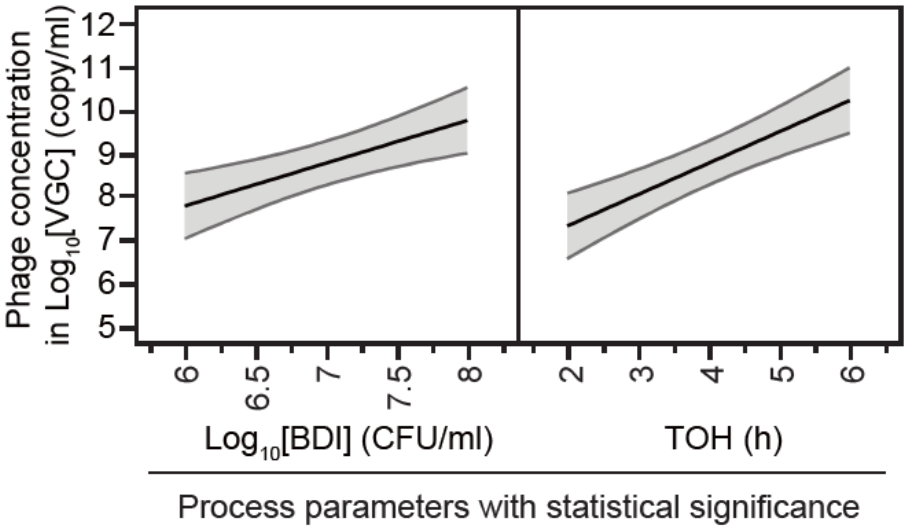


| Effect | Estimate | Standard error | *t* ratio | *P* value |
|---|---|---|---|---|
| $Log_{10}$[BDI] | 0.98 | 0.26 | 3.78 | 0.002 |
| TOH | 0.72 | 0.13 | 5.54 | <0.0001 |

**Figure 19 Interaction profiles of the regression model of phage S25-3 propagation ($Log_{10}$[VGC]).**

In the regression models of phage S25-3 propagation, phage concentrations were analyzed in $Log_{10}$[VGC]. In the top panels, the interaction plots of phage concentration with process parameters detected in the regression models are shown. In the interaction plots, the line segments with gray areas are shown as possible interactions with 95% confidence. On the bottom, the process parameters that interacted with phage concentrations with statistical significance are shown as a table. In the table, the results provided by regression analysis, including *P* values, are shown.

### 3.3.6 Comparison of propagation processes of phages S13′ and S25-3

The phage propagation of phage S13′ was compared with that of phage S25-3 using the generated models in $Log_{10}$[titer] and $Log_{10}$[VGC]. Because the $Log_{10}$[BDI] and TOH were the common parameters in the regression models of both phages S13′ and S25-3 in $Log_{10}$[titer] and $Log_{10}$[VGC], the regression models of phages S13′ and S25-3 in $Log_{10}$[titer] and $Log_{10}$[VGC] were compared using contour plots relative to these parameters (Figure 20).

Observing the contour plots, the propagation of phage S13′ was compared with that of phage S25-3, focusing on the effects of $Log_{10}$[BDI] and TOH. First, in the contour plot of phage concentrations in $Log_{10}$[titer], different patterns of the contour line at 10 of $Log_{10}$[titer] were observed between phages S13′ and S25-3, while similar patterns of contour lines were observed at 8 and 9 of $Log_{10}$[titer] (Figure 20A). Moreover, in the contour plot of phage concentrations in $Log_{10}$[VGC], similar patterns of contour lines were observed, while the concentrations of phage S13′ were one order of magnitude higher than those of phage S25-3 (Figure 20B). Thus, the propagation of phages S13′ and S25-3 had different profiles in the regression models of phage concentrations in $Log_{10}$[titer] and $Log_{10}$[VGC].

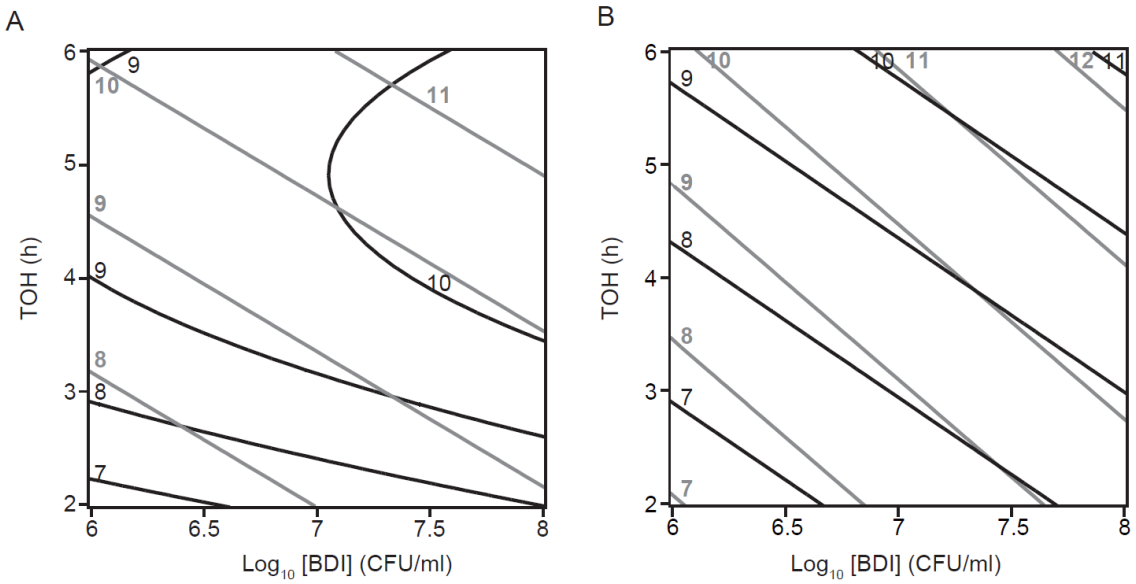


**Figure 20 Comparison of regression models of phage S13′ concentration with those of phage S25-3 using overlaid contour plots.**

The regression model of phage concentrations in (A) $Log_{10}$[titer] and (B) $Log_{10}$[VGC] were described on the contour plots relative to TOH and $Log_{10}$[BDI]. Gray and black lines show phages S13′ and S25-3, respectively. Each contour line shows the phage concentration in $Log_{10}$[titer] or $Log_{10}$[VGC].

## 3.4 Discussion

The results of phage culture experiments showed that the characteristics of the propagation process were different in phages S13′ and S25-3 (Table 7). Both regression models of phage S13′ concentrations in $Log_{10}$[titer] and $Log_{10}$[VGC] seemed to be similar, and the effects of $Log_{10}$[BDI] and TOH were critical for phage S13′ propagation (Figure 16 and Figure 17). The importance of $Log_{10}$[BDI] was previously introduced by González-Menéndez et al. in the propagation of *S. aureus* phage vB_SauM-phiIPLA-RODI (81). The criticality of TOH for phage propagation was also demonstrated, as the elapsed time was integrated into the kinetic models of phage propagation (64). On the other hand, the regression model of phage S25-3 propagation in $Log_{10}$[titer] was not compatible with that in $Log_{10}$[VGC] (Figure 18 and Figure 19). The effects of $Log_{10}$[MOI] and temperature were only observed in the regression model of phage S25-3 propagation in $Log_{10}$[titer], and the variation of TOH affected the value of $Log_{10}$[titer] and $Log_{10}$[VGC] differently. These incompatibilities of $Log_{10}$[MOI], temperature, and TOH were assumed due to the following reasons. First, because phage S25-3 possesses a relatively lower efficiency of infectious process (i.e., adsorption, latent period, and burst size) than phage S13′ on *S. aureus* strain SA27 (Figure 13), the numbers of initial phages significantly contributed to the value of $Log_{10}$[titer] at the harvest, but they were not detected in $Log_{10}$[VGC]. Second, the negative effect of temperature at the range from 34°C to 40°C was only observed for $Log_{10}$[titer], which was in agreement with the previous study on the propagation of *S. aureus* phage K, which is closely related to phage S25-3 (83). Because the effect of temperature was not detected in $Log_{10}$[VGC], only the number of active phages might be negatively impacted by higher temperature, probably due to protein misfolding and inefficient virion protein assembly at a high efficiency of host metabolism (85). Third, the positive effect of TOH was saturated at longer time periods (> 4 h) in $Log_{10}$[titer], but not in $Log_{10}$[VGC]. Because it has been reported that the concentration of viral particles influences aggregation formation of viruses, the steady

state of phage titer at > 4 h of TOH might be related to aggregation of phage particles caused by the increase of phage density (86). Thus, the results of this study revealed that the key process parameters for the propagation process differed by phage types and methodologies for counts of phage concentration.

**Table 7 Summary of the effect by process parameters.**

| Process Parameters | Phage S13′ | | Phage S25-3 | |
|---|---|---|---|---|
| | Titer (PFU/ml) | VGC (copy/ml) | Titer (PFU/ml) | VGC (copy/ml) |
| MOI | N/A | N/A | Positive | N/A |
| BDI (CFU/ml) | Positive | Positive | Positive | Positive |
| TOH (h) | Positive | Positive | Positive | Positive |
| Temperature (°C) | N/A | N/A | Negative | N/A |

From the concept of the QbD approach, it is important to evaluate and understand the effects of process parameters in the process development with statistical tools such as DoE. In this study, DSD, a new class of design of experiment, was applied and the application of DSD was considered to be quite useful in the process development of phage propagation. In this process development, relatively large numbers of experiments are considered to be required. This study suggested that phage propagation should be studied individually in each phage having different characteristics. Because the application of DSD has enabled the generation of models to understand the characteristics of the biological process with a small number of experiments, DSD contributes to a faster process development for phage manufacturing (87, 88).

Following the points mentioned above, phage culture experiments were designed and analyzed by DSD for the first time, using two *S. aureus* phages S13′ and S25-3 with different taxonomies in this study. Since the results of this study showed that the effects of process parameters differed according to the characteristics of the phages and the methodologies for phage concentration measurements (i.e., the plaque assay and qPCR), the propagation process was deemed to be studied by phage types. Thus, the choice of methodologies for phage concentration measurements needs to be considered carefully.

In conclusion, the results of this study demonstrated that the optimal propagation processes of phages could differ according to phage types and the methodologies chosen for phage concentration measurements. The knowledge obtained from this study will lead to further studies toward the establishment of manufacturing processes for *S. aureus* phages.

# CHAPTER 4 GENERAL DISCUSSION

In order to realize the manufacturing of *S. aureus* phages, a series of studies were conducted under the concept of QbD approach. ΦSA012, one of promising candidates for phage therapy, was characterized in Chapter 2. The genomic analysis by whole-genome sequencing revealed the fundamental character of ΦSA012. It was also demonstrated that ORF103 and OFR105 are RBPs of ΦSA012, which are the critical components for the host range of phages. The knowledge obtained from characterization of ΦSA012 contributes to understand the character of related phages belonging to the genus *Kayvirus*. In Chapter 3, propagation processes of *S. aureus* phages were studied in a flask with DSD using *S. aureus* phages S13′ and S25-3 in different taxonomies (the genera *Rosenblumvirus* and *Kayvirus*). As a result, phage propagation measured using the plaque assay and qPCR were overall similar to each other in the case of phage S13′, while they differed in the case of phage S25-3. These results suggest that the propagation processes need to be developed according to phage type, and the choice of methodologies for phage concentration measurements should be carefully considered. The findings in this study accelerate the establishment of phage manufacturing because the numbers of studies in process development could be minimized by focusing on key process parameters identified in this study.

To industrialize the phage therapy, establishment of the manufacturing of phages at GMP level is one of the points to be considered. Whole-genome sequencing is a useful tool to understand the nature of phages as applied in this study, and could be used as a part of the release tests in the manufacturing of phages. To maximize the inputs from whole-genome sequences of phages, it is important to accumulate the knowledge for the linkage between phenotypes and genotypes such as the identification of RBPs at the genomic level revealed in this study. Further characterization of phages is helpful to discuss the determination of CQAs and the quality control in the manufacturing. In addition, several types of phages are needed to be manufactured for one product because

the narrow spectrum of phages against bacteria should be covered by combination of different types of phages as cocktail. Since the optimal conditions for propagation process differ in types of phages, it is important to characterize phages not only for the quality control but also for process development of phage manufacturing. Considering the higher titer in the propagation process and similarity of the results measured by the plaque assay and qPCR, phage S13′ is more preferable for the manufacturing than phage S25-3. For the manufacturing of phage S25-3, the difference in the values measured by the plaque assay and qPCR should be carefully considered for the quality control. The different characters in phages S13′ and S25-3 on propagation processes could be explained by the larger size of virus particles in phages S25-3 than S13′, which could increase the higher tendency of aggregation and misfolding. Nevertheless, the key factors to determine the phages preferable for the manufacturing should be investigated furthermore. Thus, it is important to understand the features of phages to select the phages from the candidates in terms of the manufacturability.

Although the knowledge obtained in this study has contributes to realize phage therapy against *S. aureus*, there are several points to be discussed for the manufacturing of phages. First, the titer of phages in the propagation process could be increased by further optimization of the propagation process apart from the process parameters. For example, host bacteria for phage propagation should be discussed as one of the elements for optimization of the propagation process. For *S. aureus* phages, the choice of host bacteria for phage manufacturing has been partially discussed as exemplified that the food-grade species *Staphylococcus xylosus* was used for host bacteria instead of *S. aureus* from the perspective of safety concerns by the toxicity of *S. aureus*. However, it has not been considered yet to optimize host bacteria to increase the phage titer (e.g., genetic engineering of host bacteria). Since the phage propagation relies on the protein expression system in host bacteria, the capability of the protein expression in host bacteria would be one of the factors to increase the titer of phages. The optimization of media for growing

host bacteria is also important to increase the phage titer because the density of host bacteria is critical to increase the phage titer, which was confirmed in this study. Second, the purification process is also needed to be studied as well as the propagation process. For the preparation of phages at laboratory-scale, CsCl density gradient centrifugation by using the ultracentrifuge is a popular method to purify the phage solutions. However, it is difficult to use the ultracentrifuge at manufacturing-scale, and it is necessary to develop the chromatographic methods for the phage purification (89, 90). Although few studies have been reported in development of the purification process for phage manufacturing, it is important to optimize the purification process furthermore, especially focusing on removal impurities (e.g., endotoxin) and increase of the yields. The optimal conditions for the purification process might be different in types of phages, which should be confirmed by further studies. Third, formulation is also required to be considered in order to assure the stability of phages for reasonable storage. Since the phage particles are the complex of proteins, optimization of formulation is required as well as other biopharmaceuticals. In addition to degradation of phage particles, aggregation of phage particles in drug product is also one of the concerns for phage therapy. As reported in the clinical trial of PhagoBurm for a burn wound infected with *Pseudomonas aeruginosa*, aggregation of phage particles decreased the titer of phages, which determines of efficacy of the products (20). Optimization of formulation buffer could improve the stability of phages as aggregation of viral particles is caused by multiple factors, such as salt concentration, pH, type, concentration of cations, etc. (86). The freeze drying (lyophilization) has been also suggested for the drug product of phages, which could avoid aggregation and degradation of phage particles (91). However, further studies in formulation are required to improve the stability of phages as the drug product.

In conclusion, the host recognition mechanism of *S. aureus* phages in the genus *Kayvirus* were revealed in this study, which could contribute to define CQAs of *S. aureus* phages. The key process parameters of *S. aureus* phages were identified in propagation

process. The knowledge obtained in this study contributes to realization of phage therapy.

# PUBLISHMENTS

Takeuchi I, Osada K, Azam AH, Asakawa H, Miyanaga K, Tanji Y. 2016. The presence of two receptor-binding proteins contributes to the wide host range of staphylococcal Twort-like phages. Appl Environ Microbiol 82: 5763-5774.

Takeuchi I, Nasukawa T, Sugimoto R, Takemura-Uchiyama I, Murakami H, Uchiyama J. 2021. Analyses of propagation processes of *Staphylococcus aureus* bacteriophages S13′ and S25-3 in two different taxonomies by definitive screening design. Virus Res 298: 198406.

# ACKNOWLEDGEMENTS

I am deeply grateful to Prof. Kouji Nakamura for thoughtful guiding in the doctoral program in University of Tsukuba.

I am deeply grateful to Prof. Motoo Utsumi, Prof. Nobuhiko Nomura, and Prof. Yuzuru Ito for the great advice during the evaluation in the doctoral program in University of Tsukuba.

I am deeply grateful to Prof. Yasunori Tanji and Assoc. Prof. Kazuhiko Miyanaga for introducing me the world of bacteriophage.

I am deeply grateful to Assoc. Prof. Jumpei Uchiyama for technical advises and heartful coaching for phage therapy.

I would like to thank my colleagues in Astellas Pharm Inc. for the insightful discussion and kind encouragement.

Finally, I would like to thank my family for their continuous encouragement and support.

# REFERENCES


1. Humphreys H. 2012. *Staphylococcus*. p. 176-182. *In* Greenwood D, Barer M, Slack R, Irving W (ed), Medical microbiology: a guide to microbial infections: pathogenesis, immunity, laboratory diagnosis and control, 18th ed. Edinburgh; New York: Churchill Livingstone/Elsevier.
2. Enright MC, Robinson DA, Randle G, Feil EJ, Grundmann H, Spratt BG. 2002. The evolutionary history of methicillin-resistant *Staphylococcus aureus* (MRSA). Proc Natl Acad Sci USA 99: 7687-7692.
3. Lee AS, de Lencastre H, Garau J, Kluytmans J, Malhotra-Kumar S, Peschel A, Harbarth S. 2018. Methicillin-resistant *Staphylococcus aureus*. Nat Rev Dis Primers 4: 18033.
4. Turner NA, Sharma-Kuinkel BK, Maskarinec SA, Eichenberger EM, Shah PP, Carugati M, Holland TL, Fowler VG, Jr. 2019. Methicillin-resistant *Staphylococcus aureus*: an overview of basic and clinical research. Nat Rev Microbiol 17: 203-218.
5. Choo EJ, Chambers HF. 2016. Treatment of methicillin-resistant *Staphylococcus aureus* bacteremia. Infect Chemother 48: 267-273.
6. O'Neill J. 2014. Antimicrobial resistance: tackling a crisis for the health and wealth of nations [webpage]. https://amr-review.org/sites/default/files/AMR%20Review%20Paper%20-%20Tackling%20a%20crisis%20for%20the%20health%20and%20wealth%20of%20nations_1.pdf. Accessed
7. WHO. 2015. Global action plan on antimicrobial resistance [webpage]. https://apps.who.int/iris/rest/bitstreams/864486/retrieve. Accessed
8. Ryan EM, Gorman SP, Donnelly RF, Gilmore BF. 2011. Recent advances in bacteriophage therapy: how delivery routes, formulation, concentration and timing influence the success of phage therapy. J Pharm Pharmacol 63: 1253-1264.

9. Chan BK, Abedon ST, Loc-Carrillo C. 2013. Phage cocktails and the future of phage therapy. Future Microbiol 8: 769-783.
10. Aslam S, Lampley E, Wooten D, Karris M, Benson C, Strathdee S, Schooley RT. 2020. Lessons learned from the first 10 consecutive cases of intravenous bacteriophage therapy to treat multidrug-resistant bacterial infections at a single center in the United States. Open Forum Infect Dis 7: ofaa389.
11. Leitner L, Ujmajuridze A, Chanishvili N, Goderdzishvili M, Chkonia I, Rigvava S, Chkhotua A, Changashvili G, McCallin S, Schneider MP. 2020. Intravesical bacteriophages for treating urinary tract infections in patients undergoing transurethral resection of the prostate: a randomised, placebo-controlled, double-blind clinical trial. Lancet Infect Dis 3099: 30330-30333.
12. Matsuzaki S, Yasuda M, Nishikawa H, Kuroda M, Ujihara T, Shuin T, Shen Y, Jin Z, Fujimoto S, Nasimuzzaman MD, Wakiguchi H, Sugihara S, Sugiura T, Koda S, Muraoka A, Imai S. 2003. Experimental protection of mice against lethal *Staphylococcus aureus* infection by novel bacteriophage phiMR11. J Infect Dis 187: 613-624.
13. Petrovic Fabijan A, Lin RCY, Ho J, Maddocks S, Ben Zakour NL, Iredell JR, Westmead Bacteriophage Therapy Team. 2020. Safety of bacteriophage therapy in severe *Staphylococcus aureus* infection. Nat Microbiol 5: 465-472.
14. Takemura-Uchiyama I, Uchiyama J, Kato S, Inoue T, Ujihara T, Ohara N, Daibata M, Matsuzaki S. 2013. Evaluating efficacy of bacteriophage therapy against *Staphylococcus aureus* infections using a silkworm larval infection model. FEMS Microbiol Lett 347: 52-60.
15. Wills QF, Kerrigan C, Soothill JS. 2005. Experimental bacteriophage protection against *Staphylococcus aureus* abscesses in a rabbit model. Antimicrob Agents Chemother 49: 1220-1221.
16. Febvre HP, Rao S, Gindin M, Goodwin NDM, Finer E, Vivanco JS, Lu S, Manter

DK, Wallace TC, Weir TL. 2019. PHAGE study: effects of supplemental bacteriophage intake on inflammation and gut microbiota in healthy adults. Nutrients 11: 666.

17. Pirnay JP, De Vos D, Verbeken G, Merabishvili M, Chanishvili N, Vaneechoutte M, Zizi M, Laire G, Lavigne R, Huys I, Van den Mooter G, Buckling A, Debarbieux L, Pouillot F, Azeredo J, Kutter E, Dublanchet A, Gorski A, Adamia R. 2011. The phage therapy paradigm: Prêt-à-Porter or Sur-mesure? Pharm Res 28: 934-937.

18. McCallin S, Alam Sarker S, Barretto C, Sultana S, Berger B, Huq S, Krause L, Bibiloni R, Schmitt B, Reuteler G, Brussow H. 2013. Safety analysis of a Russian phage cocktail: from metagenomic analysis to oral application in healthy human subjects. Virology 443: 187-196.

19. Patey O, McCallin S, Mazure H, Liddle M, Smithyman A, Dublanchet A. 2018. Clinical Indications and Compassionate Use of Phage Therapy: Personal Experience and Literature Review with a Focus on Osteoarticular Infections. Viruses 11.

20. Jault P, Leclerc T, Jennes S, Pirnay JP, Que YA, Resch G, Rousseau AF, Ravat F, Carsin H, Le Floch R, Schaal JV, Soler C, Fevre C, Arnaud I, Bretaudeau L, Gabard J. 2019. Efficacy and tolerability of a cocktail of bacteriophages to treat burn wounds infected by *Pseudomonas aeruginosa* (PhagoBurn): a randomised, controlled, double-blind phase 1/2 trial. Lancet Infect Dis 19: 35-45.

21. Bretaudeau L, Tremblais K, Aubrit F, Meichenin M, Arnaud I. 2020. Good manufacturing practice (GMP) compliance for phage therapy medicinal products. Front Microbiol 11: 1161.

22. Mutti M, Corsini L. 2019. Robust approaches for the production of active ingredient and drug product for human phage therapy. Front Microbiol 10: 2289.

23. Finkler C, Krummen L. 2016. Introduction to the application of QbD principles

for the development of monoclonal antibodies. Biologicals 44: 282-290.

24. Mishra V, Thakur S, Patil A, Shukla A. 2018. Quality by design (QbD) approaches in current pharmaceutical set-up. Expert Opin Drug Deliv 15: 737-758.

25. Wang B, Bowles-Welch AC, Yeago C, Roy K. 2022. Process analytical technologies in cell therapy manufacturing: state-of-the-art and future directions. Adv Manuf Process 4: e10106.

26. Tustian AD, Bak H. 2021. Assessment of quality attributes for adeno-associated viral vectors. Biotechnol Bioeng 118: 4186-4203.

27. Synnott AJ, Kuang Y, Kurimoto M, Yamamichi K, Iwano H, Tanji Y. 2009. Isolation from sewage influent and characterization of novel *Staphylococcus aureus* bacteriophages with wide host ranges and potent lytic capabilities. Appl Environ Microbiol 75: 4483-4490.

28. Kreiswirth BN, Lofdahl S, Betley MJ, O'Reilly M, Schlievert PM, Bergdoll MS, Novick RP. 1983. The toxic shock syndrome exotoxin structural gene is not detectably transmitted by a prophage. Nature 305: 709-712.

29. Osada K, Takeuchi I, Miyanaga K, Tanji Y. 2017. Coevolution between *Staphylococcus aureus* isolated from mastitic milk and its lytic bacteriophage ΦSA012 in batch co-culture with serial transfer. Biochem Eng J 126: 16-23.

30. Bae T, Schneewind O. 2006. Allelic replacement in *Staphylococcus aureus* with inducible counter-selection. Plasmid 55: 58-63.

31. Carlson K. 2005. Working with bacteriophages: common techniques and methodological approaches. p. 437-494. *In* Kutter E, Sulakvelidze A (ed), Bacteriophages: biology and applications. CRC press, Boca Raton, FL, USA.

32. Altschul SF, Gish W, Miller W, Myers EW, Lipman DJ. 1990. Basic local alignment search tool. J Mol Biol 215: 403-410.

33. Lowe TM, Eddy SR. 1997. tRNAscan-SE: a program for improved detection of transfer RNA genes in genomic sequence. Nucleic Acids Res 25: 955-964.

34. Laslett D, Canback B. 2004. ARAGORN, a program to detect tRNA genes and tmRNA genes in nucleotide sequences. Nucleic Acids Res 32: 11-16.

35. Schenk S, Laddaga RA. 1992. Improved method for electroporation of *Staphylococcus aureus*. FEMS Microbiol Lett 73: 133-138.

36. Lee CY, Buranen SL, Ye ZH. 1991. Construction of single-copy integration vectors for *Staphylococcus aureus*. Gene 103: 101-105.

37. Jeong DW, Cho H, Lee H, Li C, Garza J, Fried M, Bae T. 2011. Identification of the P3 promoter and distinct roles of the two promoters of the SaeRS two-component system in *Staphylococcus aureus*. J Bacteriol 193: 4672-4684.

38. Yao J, Zhong J, Fang Y, Geisinger E, Novick RP, Lambowitz AM. 2006. Use of targetrons to disrupt essential and nonessential genes in *Staphylococcus aureus* reveals temperature sensitivity of Ll.LtrB group II intron splicing. RNA 12: 1271-1281.

39. Uchiyama J, Takemura-Uchiyama I, Kato S, Sato M, Ujihara T, Matsui H, Hanaki H, Daibata M, Matsuzaki S. 2014. *In silico* analysis of AHJD-like viruses, *Staphylococcus aureus* phages S24-1 and S13', and study of phage S24-1 adsorption. MicrobiologyOpen 3: 257-270.

40. Baptista C, Santos MA, Sao-Jose C. 2008. Phage SPP1 reversible adsorption to *Bacillus subtilis* cell wall teichoic acids accelerates virus recognition of membrane receptor YueB. J Bacteriol 190: 4989-4996.

41. Azam AH, Hoshiga F, Takeuchi I, Miyanaga K, Tanji Y. 2018. Analysis of phage resistance in *Staphylococcus aureus* SA003 reveals different binding mechanisms for the closely related Twort-like phages SA012 and SA039. Appl Microbiol Biotechnol 102: 8963-8977.

42. Stewart CR, Gaslightwala I, Hinata K, Krolikowski KA, Needleman DS, Peng AS, Peterman MA, Tobias A, Wei P. 1998. Genes and regulatory sites of the "host-takeover module" in the terminal redundancy of *Bacillus subtilis* bacteriophage

SPO1. Virology 246: 329-340.

43. Łobocka M, Hejnowicz MS, Dąbrowski K, Gozdek A, Kosakowski J, Witkowska M, Ulatowska MI, Weber-Dąbrowska B, Kwiatek M, Parasion S, Gawor J, Kosowska H, Głowacka A. 2012. Genomics of staphylococcal twort-like phages - potential therapeutics of the post-antibiotic era. p. 143-216, Advances in Virus Research, vol 83. Academic Press.

44. Alcorlo M, Gonzalez-Huici V, Hermoso JM, Meijer WJ, Salas M. 2007. The phage phi29 membrane protein p16.7, involved in DNA replication, is required for efficient ejection of the viral genome. J Bacteriol 189: 5542-5549.

45. Fraser JS, Yu Z, Maxwell KL, Davidson AR. 2006. Ig-like domains on bacteriophages: a tale of promiscuity and deceit. J Mol Biol 359: 496-507.

46. Fraser JS, Maxwell KL, Davidson AR. 2007. Immunoglobulin-like domains on bacteriophage: weapons of modest damage? Curr Opin Microbiol 10: 382-387.

47. Samson JE, Magadan AH, Sabri M, Moineau S. 2013. Revenge of the phages: defeating bacterial defences. Nat Rev Microbiol 11: 675-687.

48. Brun E, Johnson PE, Creagh AL, Tomme P, Webster P, Haynes CA, McIntosh LP. 2000. Structure and binding specificity of the second N-terminal cellulose-binding domain from *Cellulomonas fimi* endoglucanase C. Biochemistry 39: 2445-2458.

49. Hunter S, Jones P, Mitchell A, Apweiler R, Attwood TK, Bateman A, Bernard T, Binns D, Bork P, Burge S, de Castro E, Coggill P, Corbett M, Das U, Daugherty L, Duquenne L, Finn RD, Fraser M, Gough J, Haft D, Hulo N, Kahn D, Kelly E, Letunic I, Lonsdale D, Lopez R, Madera M, Maslen J, McAnulla C, McDowall J, McMenamin C, Mi H, Mutowo-Muellenet P, Mulder N, Natale D, Orengo C, Pesseat S, Punta M, Quinn AF, Rivoire C, Sangrador-Vegas A, Selengut JD, Sigrist CJ, Scheremetjew M, Tate J, Thimmajanarthanan M, Thomas PD, Wu CH, Yeats C, Yong SY. 2012. InterPro in 2011: new developments in the family and domain prediction database. Nucleic Acids Res 40: D306-312.

50. Eyer L, Pantucek R, Zdrahal Z, Konecna H, Kasparek P, Ruzickova V, Hernychova L, Preisler J, Doskar J. 2007. Structural protein analysis of the polyvalent staphylococcal bacteriophage 812. Proteomics 7: 64-72.

51. Habann M, Leiman PG, Vandersteegen K, Van den Bossche A, Lavigne R, Shneider MM, Bielmann R, Eugster MR, Loessner MJ, Klumpp J. 2014. *Listeria* phage A511, a model for the contractile tail machineries of SPO1-related bacteriophages. Mol Microbiol 92: 84-99.

52. Ohtsubo Y, Ikeda-Ohtsubo W, Nagata Y, Tsuda M. 2008. GenomeMatcher: a graphical user interface for DNA sequence comparison. BMC Bioinform 9: 376.

53. Xia G, Maier L, Sanchez-Carballo P, Li M, Otto M, Holst O, Peschel A. 2010. Glycosylation of wall teichoic acid in *Staphylococcus aureus* by TarM. J Biol Chem 285: 13405-13415.

54. Lavigne R, Darius P, Summer EJ, Seto D, Mahadevan P, Nilsson AS, Ackermann HW, Kropinski AM. 2009. Classification of *Myoviridae* bacteriophages using protein sequence similarity. BMC Microbiol 9: 224-224.

55. Schwarzer D, Buettner FFR, Browning C, Nazarov S, Rabsch W, Bethe A, Oberbeck A, Bowman VD, Stummeyer K, Muhlenhoff M, Leiman PG, Gerardy-Schahn R. 2012. A multivalent adsorption apparatus explains the broad host range of phage phi92: a comprehensive genomic and structural analysis. J Virol 86: 10384-10398.

56. Golomidova A, Kulikov E, Prokhorov N, Guerrero-Ferreira R, Knirel Y, Kostryukova E, Tarasyan K, Letarov A. 2016. Branched lateral tail fiber organization in T5-like bacteriophages DT57C and DT571/2 is revealed by genetic and functional analysis. Viruses 8: 26-26.

57. Legrand P, Collins B, Blangy S, Murphy J, Spinelli S, Gutierrez C, Richet N, Kellenberger C, Desmyter A, Mahony J, van Sinderen D, Cambillau C. 2016. The atomic structure of the phage Tuc2009 baseplate tripod suggests that host

recognition involves two different carbohydrate binding modules. mBio 7: e01781-01715.

58. Collins B, Bebeacua C, Mahony J, Blangy S, Douillard FP, Veesler D, Cambillau C, van Sinderen D. 2013. Structure and functional analysis of the host recognition device of lactococcal phage Tuc2009. J Virol 87: 8429-8440.

59. Li X, Gerlach D, Du X, Larsen J, Stegger M, Kühner P, Peschel A, Xia G, Winstel V. 2015. An accessory wall teichoic acid glycosyltransferase protects *Staphylococcus aureus* from the lytic activity of *Podoviridae*. Sci Rep 5: 17219-17219.

60. Xia G, Corrigan RM, Winstel V, Goerke C, Grundling A, Peschel A. 2011. Wall teichoic acid-dependent adsorption of staphylococcal siphovirus and myovirus. J Bacteriol 193: 4006-4009.

61. Azam AH, Tanji Y. 2019. Peculiarities of *Staphylococcus aureus* phages and their possible application in phage therapy. Appl Microbiol Biotechnol 103: 4279-4289.

62. Uchiyama J, Taniguchi M, Kurokawa K, Takemura-Uchiyama I, Ujihara T, Shimakura H, Sakaguchi Y, Murakami H, Sakaguchi M, Matsuzaki S. 2017. Adsorption of *Staphylococcus* viruses S13' and S24-1 on *Staphylococcus aureus* strains with different glycosidic linkage patterns of wall teichoic acids. J Gen Virol 98: 2171-2180.

63. Lehman SM, Mearns G, Rankin D, Cole RA, Smrekar F, Branston SD, Morales S. 2019. Design and preclinical development of a phage product for the treatment of antibiotic-resistant *Staphylococcus aureus* infections. Viruses 11: 88.

64. Garcia R, Latz S, Romero J, Higuera G, Garcia K, Bastias R. 2019. Bacteriophage production models: an overview. Front Microbiol 10: 1187.

65. Jurač K, Nabergoj D, Podgornik A. 2019. Bacteriophage production processes. Appl Microbiol Biotechnol 103: 685-694.

66. Santos SB, Carvalho C, Azeredo J, Ferreira EC. 2014. Population dynamics of a

*Salmonella* lytic phage and its host: implications of the host bacterial growth rate in modelling. PLoS One 9: e102507.

67. Mojica KD, Brussaard CP. 2014. Factors affecting virus dynamics and microbial host-virus interactions in marine environments. FEMS Microbiol Ecol 89: 495-515.

68. Warner CM, Barker N, Lee SW, Perkins EJ. 2014. M13 bacteriophage production for large-scale applications. Bioprocess Biosyst Eng 37: 2067-2072.

69. Tokman JI, Kent DJ, Wiedmann M, Denes T. 2016. Temperature significantly affects the plaquing and adsorption efficiencies of *Listeria* phages. Front Microbiol 7: 631.

70. Anderson B, Rashid MH, Carter C, Pasternack G, Rajanna C, Revazishvili T, Dean T, Senecal A, Sulakvelidze A. 2011. Enumeration of bacteriophage particles: comparative analysis of the traditional plaque assay and real-time QPCR- and nanosight-based assays. Bacteriophage 1: 86-93.

71. Jones B, Nachtsheim CJ. 2011. A class of three-level designs for definitive screening in the presence of second-order effects. J Qual Technol 43: 1-15.

72. Kropinski AM, Mazzocco A, Waddell TE, Lingohr E, Johnson RP. 2009. Enumeration of bacteriophages by double agar overlay plaque assay. Methods Mol Biol 501: 69-76.

73. Green MR, Sambrook J. 2016. Precipitation of DNA with ethanol. Cold Spring Harb Protoc 2016: 1116-1120.

74. Green MR, Sambrook J. 2017. Isolation of high-molecular-weight DNA using organic solvents. Cold Spring Harb Protoc 2017: 356-359.

75. Takemura-Uchiyama I, Uchiyama J, Kato S, Ujihara T, Daibata M, Matsuzaki S. 2014. Genomic and phylogenetic traits of *Staphylococcus* phages S25-3 and S25-4 (family *Myoviridae*, genus Twort-like viruses). Ann Microbiol 64: 1453-1456.

76. Errore A, Jones B, Li W, Nachtsheim CJ. 2017. Using definitive screening designs

to identify active first-and second-order factor effects. J Qual Technol 49: 244-264.

77. Lindeberger C, Pflug L, Huebner H, Buchholz R. 2012. A novel model for studying baculovirus infection process. Biotechnol Bioprocess Eng 17: 211-217.

78. Vicente T, Roldão A, Peixoto C, Carrondo MJ, Alves PM. 2011. Large-scale production and purification of VLP-based vaccines. J Invertebr Pathol 107 Suppl: S42-S48.

79. Postollec F, Falentin H, Pavan S, Combrisson J, Sohier D. 2011. Recent advances in quantitative PCR (qPCR) applications in food microbiology. Food Microbiol 28: 848-861.

80. Grieco SH, Wong AY, Dunbar WS, MacGillivray RT, Curtis SB. 2012. Optimization of fermentation parameters in phage production using response surface methodology. J Ind Microbiol Biotechnol 39: 1515-1522.

81. González-Menéndez E, Arroyo-López FN, Martínez B, García P, Garrido-Fernández A, Rodríguez A. 2018. Optimizing propagation of *Staphylococcus aureus* infecting bacteriophage vB_sauM-phiIPLA-RODI on *Staphylococcus xylosus* using response surface methodology. Viruses 10: 153.

82. Agboluaje M, Sauvageau D. 2018. Bacteriophage production in bioreactors. Methods Mol Biol 1693: 173-193.

83. Ali J, Rafiq Q, Ratcliffe E. 2019. A scaled-down model for the translation of bacteriophage culture to manufacturing scale. Biotechnol Bioeng 116: 972-984.

84. Jones B, Nachtsheim CJ. 2017. Effective design-based model selection for definitive screening designs. Technometrics 59: 319-329.

85. Baneyx F, Mujacic M. 2004. Recombinant protein folding and misfolding in *Escherichia coli*. Nat Biotechnol 22: 1399-1408.

86. Gerba CP, Betancourt WQ. 2017. Viral aggregation: impact on virus behavior in the environment. Environ Sci Technol 51: 7318-7325.

87. Tai M, Ly A, Leung I, Nayar G. 2015. Efficient high-throughput biological process characterization: definitive screening design with the ambr250 bioreactor system. Biotechnol Prog 31: 1388-1395.

88. Hocharoen L, Noppiboon S, Kitsubun P. 2020. Process characterization by definitive screening design approach on DNA vaccine production. Front Bioeng Biotechnol 15: 574809.

89. Bourdin G, Schmitt B, Marvin Guy L, Germond JE, Zuber S, Michot L, Reuteler G, Brussow H. 2014. Amplification and purification of T4-like escherichia coli phages for phage therapy: from laboratory to pilot scale. Appl Environ Microbiol 80: 1469-1476.

90. Smrekar F, Ciringer M, Jančar J, Raspor P, Štrancar A, Podgornik A. 2011. Optimization of lytic phage manufacturing in bioreactor using monolithic supports. J Sep Sci 34: 2152-2158.

91. Malik DJ, Sokolov IJ, Vinner GK, Mancuso F, Cinquerrui S, Vladisavljevic GT, Clokie MRJ, Garton NJ, Stapley AGF, Kirpichnikova A. 2017. Formulation, stabilisation and encapsulation of bacteriophage for phage therapy. Adv Colloid Interface Sci 249: 100-133.

# APPENDIX

General features of all putative ORFs from ΦSA012

| ORF | bp | | Length | predicted function |
|---|---|---|---|---|
| | start | stop | (aa) | |
| 1 | 14 | 484 | 156 | terminal repeat-encoded protein |
| 2 | 543 | 716 | 57 | terminal repeat-encoded protein |
| 3 | 716 | 982 | 88 | terminal repeat-encoded protein |
| 4 | 1067 | 1246 | 59 | terminal repeat-encoded protein |
| 5 | 1817 | 1581 | 78 | border ORF L protein,unknown function |
| 6 | 2251 | 1817 | 144 | N/A |
| 7 | 2445 | 2254 | 63 | putative membrane protein |
| 8 | 2927 | 2442 | 161 | membrane protein |
| 9 | 3351 | 2920 | 143 | N/A |
| 10 | 3907 | 3365 | 180 | N/A |
| 11 | 4407 | 3919 | 162 | N/A |
| 12 | 4875 | 4468 | 135 | N/A |
| 13 | 5588 | 4878 | 236 | serine/threonine protein phosphatase |
| 14 | 7552 | 5684 | 622 | N/A |
| 15 | 9008 | 8460 | 182 | N/A |
| 16 | 9230 | 9012 | 72 | N/A |
| 17 | 9425 | 9231 | 64 | N/A |
| 18 | 10152 | 9415 | 245 | N/A |
| 19 | 10570 | 10331 | 79 | N/A |
| 20 | 10961 | 10572 | 129 | N/A |
| 21 | 11232 | 11059 | 57 | N/A |
| 22 | 11755 | 11273 | 160 | N/A |
| 23 | 12347 | 11805 | 180 | N/A |
| 24 | 12880 | 12347 | 177 | N/A |
| 25 | 13047 | 12883 | 54 | putative membrane protein |
| 26 | 13328 | 13050 | 92 | putative membrane protein |
| 27 | 14173 | 13328 | 281 | N/A |
| 28 | 15303 | 14185 | 372 | AAA family ATPase |
| 29 | 15782 | 15456 | 108 | N/A |
| 30 | 16191 | 15775 | 138 | N/A |
| 31 | 16626 | 16324 | 100 | DNA binding protein |
| 32 | 16814 | 16626 | 62 | N/A |
| 33 | 17019 | 16858 | 53 | N/A |
| 34 | 19067 | 17019 | 682 | N/A |
| 35 | 19408 | 19145 | 87 | virion component |
| 36 | 19598 | 19425 | 57 | N/A |
| 37 | 20183 | 19605 | 192 | membrane protein |
| 38 | 20802 | 20176 | 208 | N/A |
| 39 | 21691 | 20795 | 298 | putative DNA ligase |
| 40 | 21915 | 21691 | 74 | putative membrane protein |
| 41 | 22724 | 21984 | 246 | PhoH-related protein |
| 42 | 23390 | 22776 | 204 | virion component |
| 43 | 23831 | 23406 | 141 | N/A |
| 44 | 24012 | 23821 | 63 | N/A |
| 45 | 24676 | 24035 | 213 | N/A |
| 46 | 24896 | 24666 | 76 | N/A |
| 47 | 25126 | 24899 | 75 | N/A |
| 48 | 25927 | 25235 | 230 | putative transglycosylase |
| 49 | 26918 | 26124 | 264 | putative membrane protein |
| 50 | 27226 | 26918 | 102 | putative membrane protein |
| 51 | 28826 | 27339 | 495 | N-acetylmuramoyl-L-alanine amidase |
| 52 | 29329 | 28826 | 167 | putative holin |
| 53 | 29599 | 29414 | 61 | N/A |
| 54 | 30269 | 29787 | 160 | HNH endonuclease |
| 55 | 31870 | 31652 | 72 | N/A |
| 56 | 32557 | 32348 | 69 | virion component |
| 57 | 32902 | 32570 | 110 | N/A |
| 58 | 33241 | 32915 | 108 | putative membrane protein |
| 59 | 33801 | 34067 | 88 | putative membrane protein |
| 60 | 34045 | 34323 | 92 | N/A |
| 61 | 34320 | 34730 | 136 | N/A |
| 62 | 34745 | 36562 | 605 | Terminase |
| 63 | 36576 | 37376 | 266 | virion component |

| | | | | |
|---|---|---|---|---|
| 64 | 37363 | 37536 | 57 | N/A |
| 65 | 37533 | 38012 | 159 | N/A |
| 66 | 38105 | 39271 | 388 | putative membrane protein |
| 67 | 39509 | 39697 | 62 | putative membrane protein |
| 68 | 39716 | 40087 | 123 | N/A |
| 69 | 40091 | 41782 | 563 | putative portal protein |
| 70 | 41976 | 42749 | 257 | putative prohead protease |
| 71 | 42768 | 43724 | 318 | N/A |
| 72 | 43840 | 45231 | 463 | putative capsid protein |
| 73 | 45323 | 45553 | 76 | hypothetical protein |
| 74 | 45566 | 46474 | 302 | putative tail fiber protein |
| 75 | 46488 | 47366 | 292 | virion component |
| 76 | 47366 | 47986 | 206 | N/A |
| 77 | 48005 | 48841 | 278 | baseplate hub assembly protein |
| 78 | 48843 | 49058 | 71 | N/A |
| 79 | 49085 | 50848 | 587 | putative major tail sheath protein |
| 80 | 50921 | 51349 | 142 | putative tail tube protein |
| 81 | 51459 | 52430 | 323 | putative intron-encoded nuclease |
| 82 | 52496 | 52654 | 52 | N/A |
| 83 | 52644 | 52781 | 45 | N/A |
| 84 | 52824 | 53276 | 150 | N/A |
| 85 | 53289 | 53483 | 64 | putative membrane protein |
| 86 | 53554 | 53865 | 103 | virion component |
| 87 | 53997 | 54455 | 152 | N/A |
| 88 | 54490 | 55035 | 181 | tail morphogenetic protein |
| 89 | 55091 | 59146 | 1351 | tail morphogenetic protein, tape masure protein |
| 90 | 59225 | 61651 | 808 | tail morphogenetic protein |
| 91 | 61665 | 62552 | 295 | tail morphogenetic protein, putative peptideglycan hydrolase |
| 92 | 62638 | 62898 | 86 | N/A |
| 93 | 62888 | 63997 | 369 | mobile element protein |
| 94 | 64193 | 66739 | 848 | putative glycerophosphoryl diester phosphodiesterase |
| 95 | 66845 | 67636 | 263 | virion component |
| 96 | 67636 | 68160 | 174 | virion component |
| 97 | 68160 | 68864 | 234 | putative baseplate protein |
| 98 | 68879 | 69925 | 348 | putative baseplate protein |
| 99 | 69946 | 73005 | 1019 | tail morphogenetic protein |
| 100 | 73116 | 73637 | 173 | putative baseplate protein |
| 101 | 73658 | 77116 | 1152 | tail morphogenetic protein (siliadase domain), putative adsorption associated tail protein |
| 102 | 77165 | 77323 | 52 | N/A |
| 103 | 77324 | 79246 | 640 | virion component |
| 104 | 79268 | 79639 | 123 | virion component |
| 105 | 79646 | 81022 | 458 | virion component |
| 106 | 81112 | 82860 | 582 | DNA helicase |
| 107 | 82872 | 84485 | 537 | putative Rep protein |
| 108 | 84478 | 85920 | 480 | DNA helicase |
| 109 | 85999 | 87024 | 341 | putative exonuclease |
| 110 | 87024 | 87401 | 125 | N/A |
| 111 | 87401 | 89320 | 639 | putative exonuclease |
| 112 | 89320 | 89916 | 198 | anti- sigma factor |
| 113 | 89931 | 90998 | 355 | DNA primase |
| 114 | 91064 | 91402 | 112 | N/A |
| 115 | 91402 | 91854 | 150 | N/A |
| 116 | 91841 | 92449 | 202 | N/A |
| 117 | 92466 | 92858 | 130 | ribonucleotide reduction protein NrdI |
| 118 | 92873 | 94987 | 704 | ribonucleotide reductase large subunit |
| 119 | 95001 | 96050 | 349 | ribonucleotide reductase minor subunit |
| 120 | 96068 | 96397 | 109 | N/A |
| 121 | 96381 | 96701 | 106 | thioredoxin-like protein |
| 122 | 96908 | 97504 | 198 | N/A |
| 123 | 97514 | 97819 | 101 | transcription factor |
| 124 | 97896 | 101114 | 1072 | DNA polymerase I |
| 125 | 101184 | 101426 | 80 | N/A |
| 126 | 101443 | 101925 | 160 | N/A |
| 127 | 102012 | 103283 | 423 | N/A |
| 128 | 103497 | 104477 | 326 | N/A |
| 129 | 104648 | 105913 | 421 | putative DNA repair protein |
| 130 | 105917 | 106270 | 117 | N/A |
| 131 | 106257 | 106919 | 220 | RNA polymerase sigma factor |
| 132 | 107046 | 107678 | 210 | putative tail morphogenetic protein |
| 133 | 107701 | 108213 | 170 | putative tail morphogenetic protein (Ig-like domain) |
| 134 | 108228 | 108455 | 75 | putative tail morphogenetic protein |

| | | | | |
|---|---|---|---|---|
| 135 | 108550 | 108810 | 86 | N/A |
| 136 | 108814 | 109569 | 251 | N/A |
| 137 | 109562 | 110812 | 416 | putative metallophosphoesterase |
| 138 | 110826 | 111194 | 122 | putative membrane protein |
| 139 | 111181 | 111492 | 103 | N/A |
| 140 | 111556 | 112092 | 178 | N/A |
| 141 | 112085 | 112852 | 255 | N/A |
| 142 | 112830 | 113276 | 148 | N/A |
| 143 | 113276 | 114139 | 287 | N/A |
| 144 | 114511 | 115242 | 243 | N/A |
| 145 | 115260 | 115718 | 152 | virion component |
| 146 | 115783 | 116226 | 147 | N/A |
| 147 | 116243 | 116947 | 234 | N/A |
| 148 | 117009 | 117407 | 132 | putative membrane protein |
| 149 | 117555 | 117797 | 80 | N/A |
| 150 | 117802 | 118359 | 185 | N/A |
| 151 | 118395 | 118571 | 58 | DNA sliding clump inhibitor,arrest of *S.aureus* DNA synthesis |
| 152 | 118564 | 118812 | 82 | hypothetical protein |
| 153 | 118805 | 119038 | 77 | hypothetical protein |
| 154 | 119119 | 119763 | 214 | putative membrane protein |
| 155 | 119778 | 120026 | 82 | putative membrane protein |
| 156 | 120038 | 120214 | 58 | N/A |
| 157 | 120207 | 120503 | 98 | N/A |
| 158 | 120551 | 120733 | 60 | putative membrane protein |
| 159 | 120746 | 121117 | 123 | N/A |
| 160 | 121130 | 121477 | 115 | N/A |
| 161 | 121477 | 121755 | 92 | putative membrane protein |
| 162 | 121825 | 122130 | 101 | N/A |
| 163 | 122145 | 122495 | 116 | N/A |
| 164 | 122495 | 123097 | 200 | N/A |
| 165 | 123111 | 123290 | 59 | N/A |
| 166 | 123517 | 123918 | 133 | putative membrane protein |
| 167 | 123920 | 124213 | 97 | N/A |
| 168 | 124230 | 124517 | 95 | putative membrane protein |
| 169 | 124637 | 125041 | 134 | N/A |
| 170 | 125046 | 125282 | 78 | N/A |
| 171 | 125279 | 125806 | 175 | phosphoesterase |
| 172 | 125787 | 126107 | 106 | N/A |
| 173 | 126107 | 126337 | 76 | N/A |
| 174 | 126850 | 127167 | 105 | N/A |
| 175 | 127168 | 127848 | 226 | virion component |
| 176 | 127926 | 128084 | 52 | putative membrane protein |
| 177 | 128100 | 128324 | 74 | N/A |
| 178 | 128337 | 128537 | 66 | N/A |
| 179 | 128538 | 128828 | 96 | putative membrane protein |
| 180 | 128922 | 129230 | 102 | N/A |
| 181 | 129227 | 130135 | 302 | putative ribose-phosphate pyrophosphokinase |
| 182 | 130153 | 131622 | 489 | nicotinamide phosphoribosyl transferase |
| 183 | 131701 | 131946 | 81 | N/A |
| 184 | 131963 | 132355 | 130 | N/A |
| 185 | 132357 | 132554 | 65 | N/A |
| 186 | 132619 | 132915 | 98 | terminal repeat-encoded protein |
| 187 | 132919 | 133230 | 103 | N/A |
| 188 | 133236 | 133535 | 99 | N/A |
| 189 | 133535 | 133774 | 79 | N/A |
| 190 | 133923 | 134168 | 81 | N/A |
| 191 | 134187 | 134573 | 128 | N/A |
| 192 | 135240 | 135533 | 97 | terminal repeat-encoded protein |
| 193 | 135530 | 135715 | 61 | terminal repeat-encoded protein |
| 194 | 135823 | 136113 | 96 | terminal repeat-encoded protein |
| 195 | 136113 | 136400 | 95 | terminal repeat-encoded protein |
| 196 | 136400 | 136696 | 98 | terminal repeat-encoded protein |
| 197 | 136700 | 136948 | 82 | terminal repeat-encoded protein |
| 198 | 137030 | 137275 | 81 | terminal repeat-encoded protein |
| 199 | 137286 | 137633 | 115 | terminal repeat-encoded protein |
| 200 | 137742 | 138350 | 202 | terminal repeat-encoded protein |
| 201 | 138892 | 138554 | 112 | terminal repeat-encoded protein |
| 202 | 139202 | 139510 | 102 | terminal repeat-encoded protein |
| 203 | 139717 | 140004 | 95 | terminal repeat-encoded protein |
| 204 | 140054 | 140245 | 63 | terminal repeat-encoded protein |
| 205 | 141088 | 141411 | 107 | terminal repeat-encoded protein |

| | | | | |
|---|---|---|---|---|
| 206 | 141486 | 141623 | 45 | N/A |
| 207 | 141694 | 141858 | 54 | N/A |